UCLouvain

AGRO LOUVAIN

Faculté des bioingénieurs

Supporting information:

Accumulation of Mono-Reduced $[Ir(piq)_2(LL)]^+$ Photosensitizers Relevant for Solar Fuels Productions

Author: Martin WODON
Supervisors: Benjamin ELIAS & Ludovic TROIAN-GAUTIER
Readers: Christine DUPONT & Sophie HERMANS
Academic year 2023–2024
Mémoire de fin d'étude en vue de l'obtention du diplôme de Bioingénieur : chimie et bio-industries

Contents

ELECTROCHEMISTRY **S3**

ADDITIONAL STERN-VOLMER PLOTS **S8**

STEADY-STATE PHOTOLYSIS **S16**

HIGH-RESOLUTION MASS SPECTROMETRY **S19**

^{1}H NMR SPECTRA **S28**

Electrochemistry

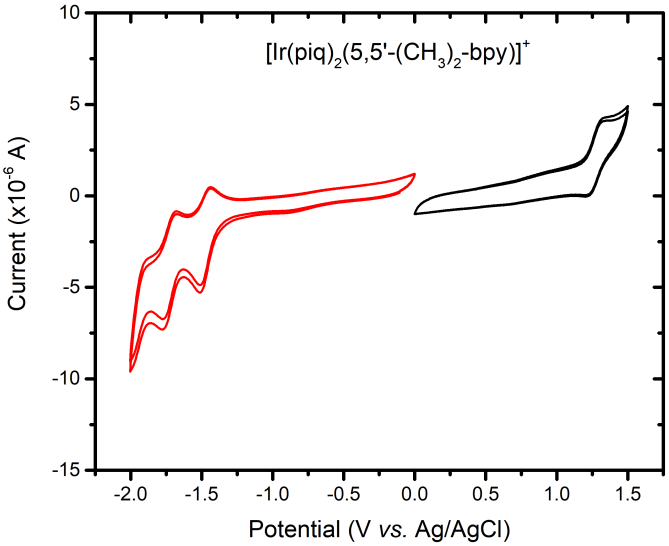

Figure S1. Cyclic voltammetry of $[Ir(piq)_2(5,5'\text{-}(CH_3)_2\text{-}bpy]^+.PF_6^-$ recorded at 100 mV/s in acetonitrile with 0.1M $TBAPF_6$ electrolyte.

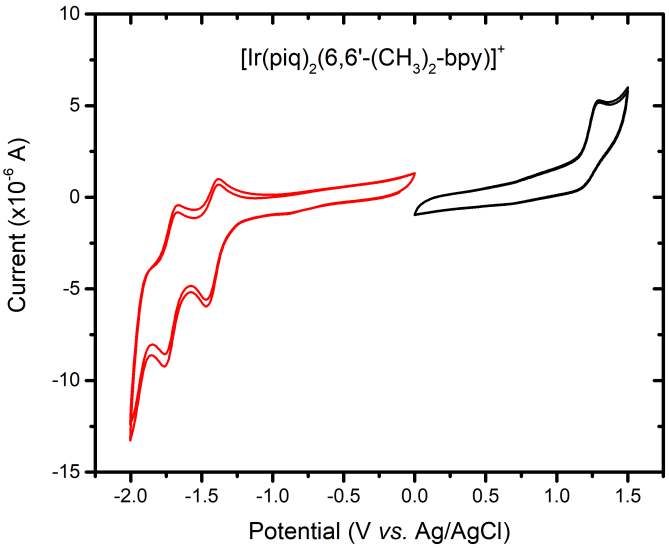

Figure S2. Cyclic voltammetry of $[Ir(piq)_2(6,6'\text{-}(CH_3)_2\text{-}bpy]^+.PF_6^-$ recorded at 100 mV/s in acetonitrile with 0.1M $TBAPF_6$ electrolyte.

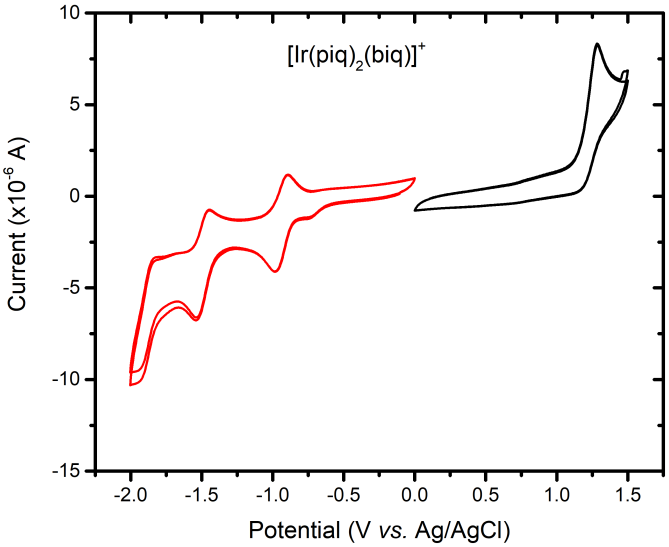

Figure S3. Cyclic voltammetry of $[Ir(piq)_2(biq)]^+.PF_6^-$ recorded at 100 mV/s in acetonitrile with 0.1M $TBAPF_6$ electrolyte.

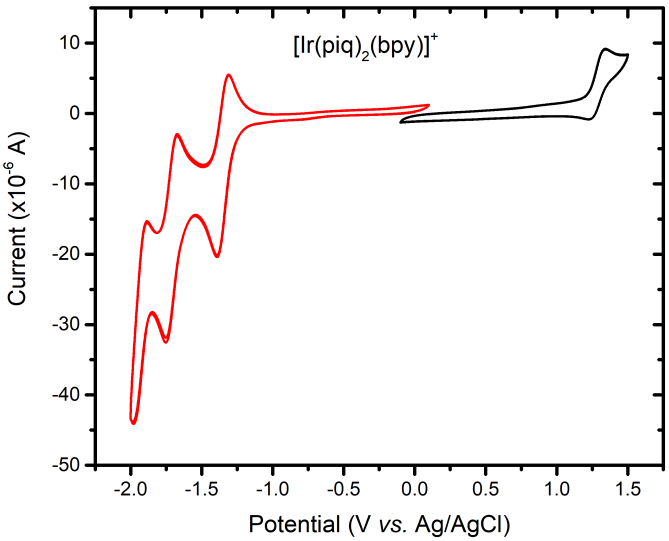

Figure S4. Cyclic voltammetry of $[Ir(piq)_2(bpy)]^+.PF_6^-$ recorded at 100 mV/s in acetonitrile with 0.1M $TBAPF_6$ electrolyte.

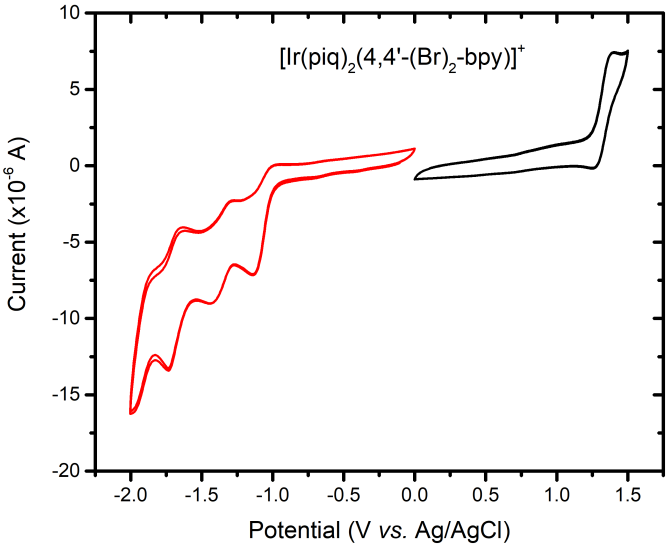

Figure S5. Cyclic voltammetry of $[Ir(piq)_2(4,4'\text{-}(Br)_2\text{-}bpy]^+.PF_6^-$ recorded at 100 mV/s in acetonitrile with 0.1M $TBAPF_6$ electrolyte.

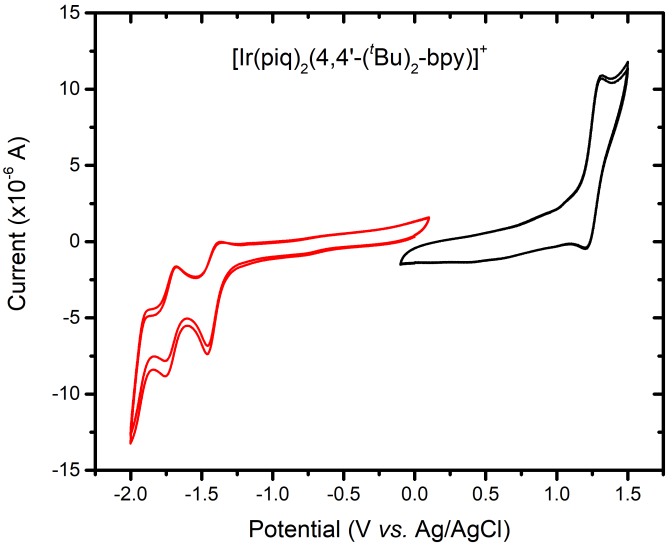

Figure S6. Cyclic voltammetry of $[Ir(piq)_2(4,4'\text{-}(^tBu)_2\text{-}bpy]^+.PF_6^-$ recorded at 100 mV/s in acetonitrile with 0.1M $TBAPF_6$ electrolyte.

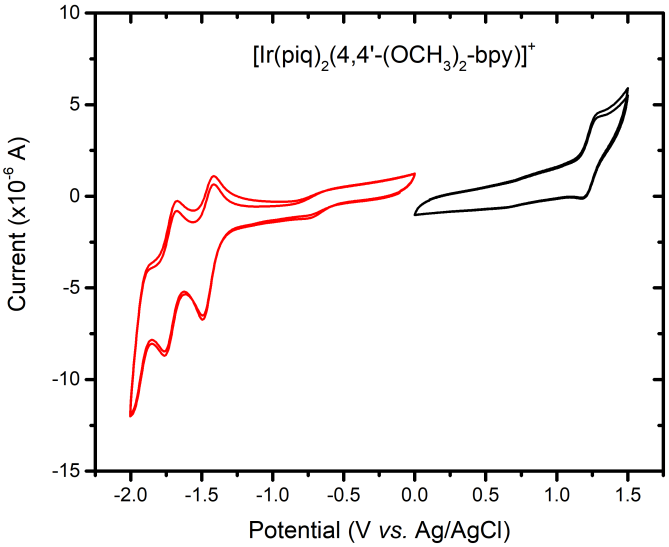

Figure S7. Cyclic voltammetry of $[Ir(piq)_2(4,4'\text{-}(OCH_3)_2\text{-}bpy]^+.PF_6^-$ recorded at 100 mV/s in acetonitrile with 0.1M $TBAPF_6$ electrolyte.

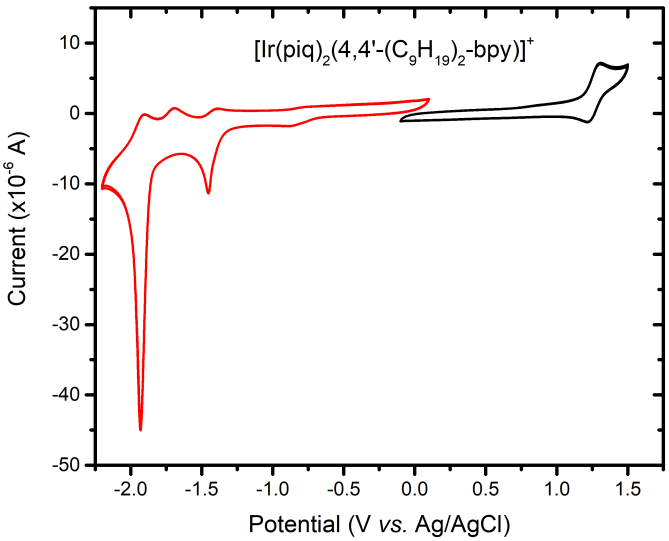

Figure S8. Cyclic voltammetry of $[Ir(piq)_2(4,4'\text{-}(C_9H_{19})_2\text{-}bpy]^+.PF_6^-$ recorded at 100 mV/s in acetonitrile with 0.1M $TBAPF_6$ electrolyte.

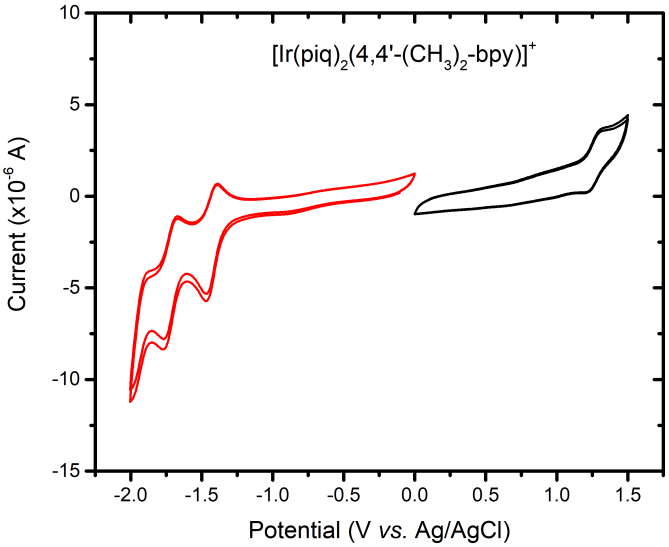

Figure S9. Cyclic voltammetry of $[Ir(piq)_2(4,4'\text{-}(CH_3)_2\text{-}bpy]^+.PF_6^-$ recorded at 100 mV/s in acetonitrile with 0.1M $TBAPF_6$ electrolyte.

Additional Stern-Volmer Plots

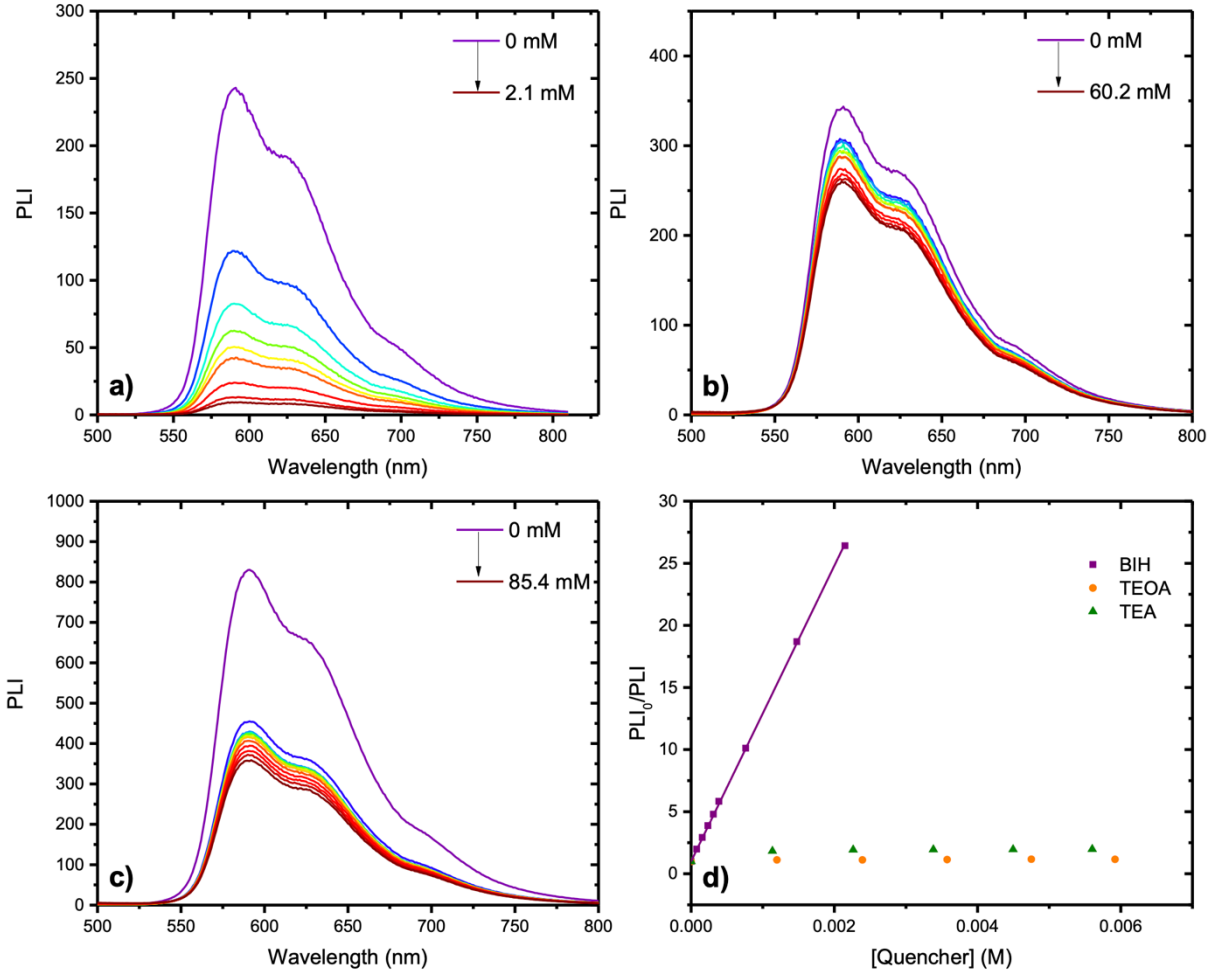

Figure S10. Excited-state quenching of $[Ir(piq)_2(4,4'\text{-}(CH_3)_2\text{-}bpy)]^+$ with BIH (a), TEOA (b) and TEA (c) in argon purged acetonitrile. The corresponding Stern-Volmer plots is shown in panel d, with the corresponding linear fit for the excited-state quenching in the presence of BIH.

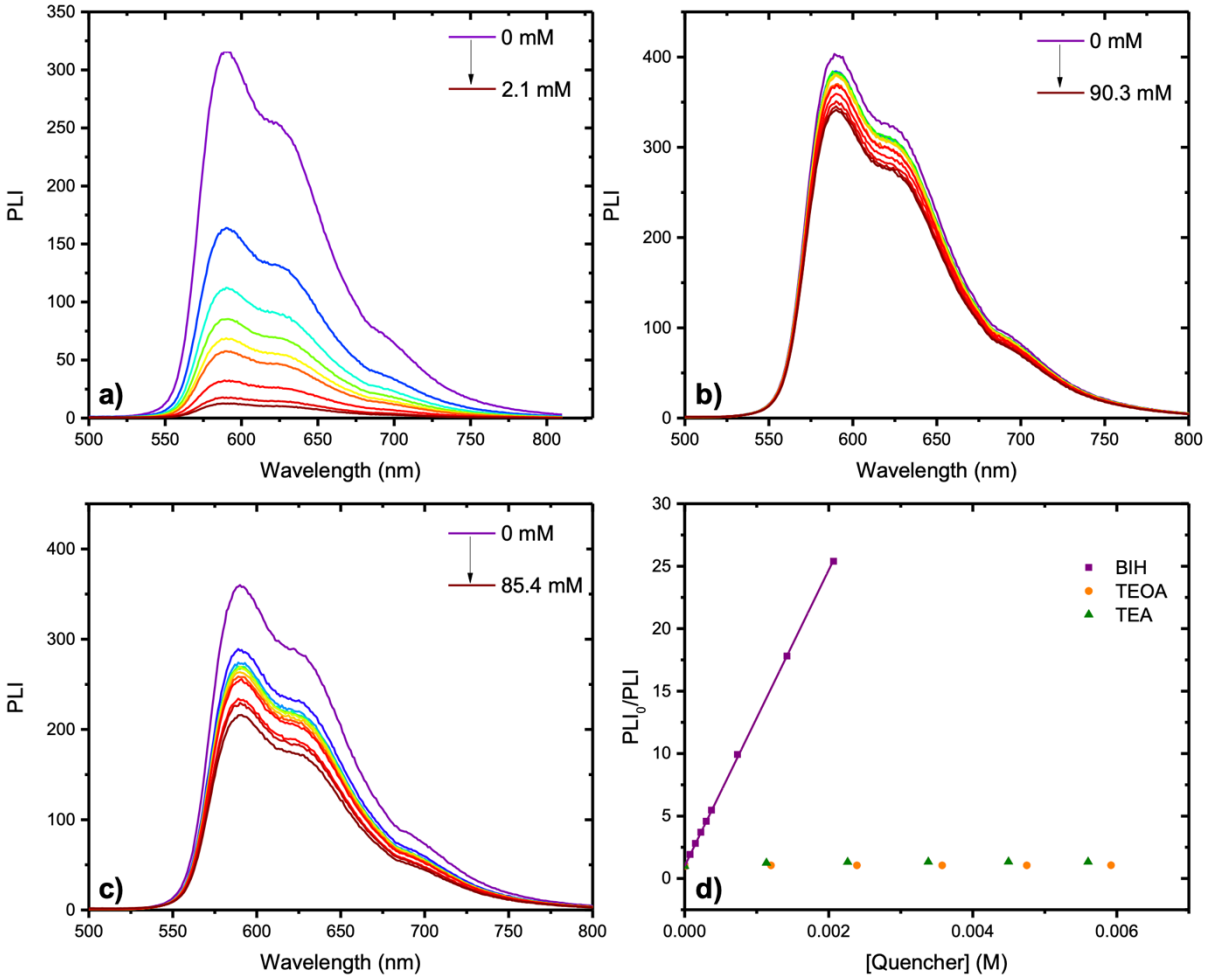

Figure S11. Excited-state quenching of $[Ir(piq)_2(5,5'\text{-}(CH_3)_2\text{-}bpy)]^+$ with BIH (a), TEOA (b) and TEA (c) in argon purged acetonitrile. The corresponding Stern-Volmer plots is shown in panel d, with the corresponding linear fit for the excited-state quenching in the presence of BIH.

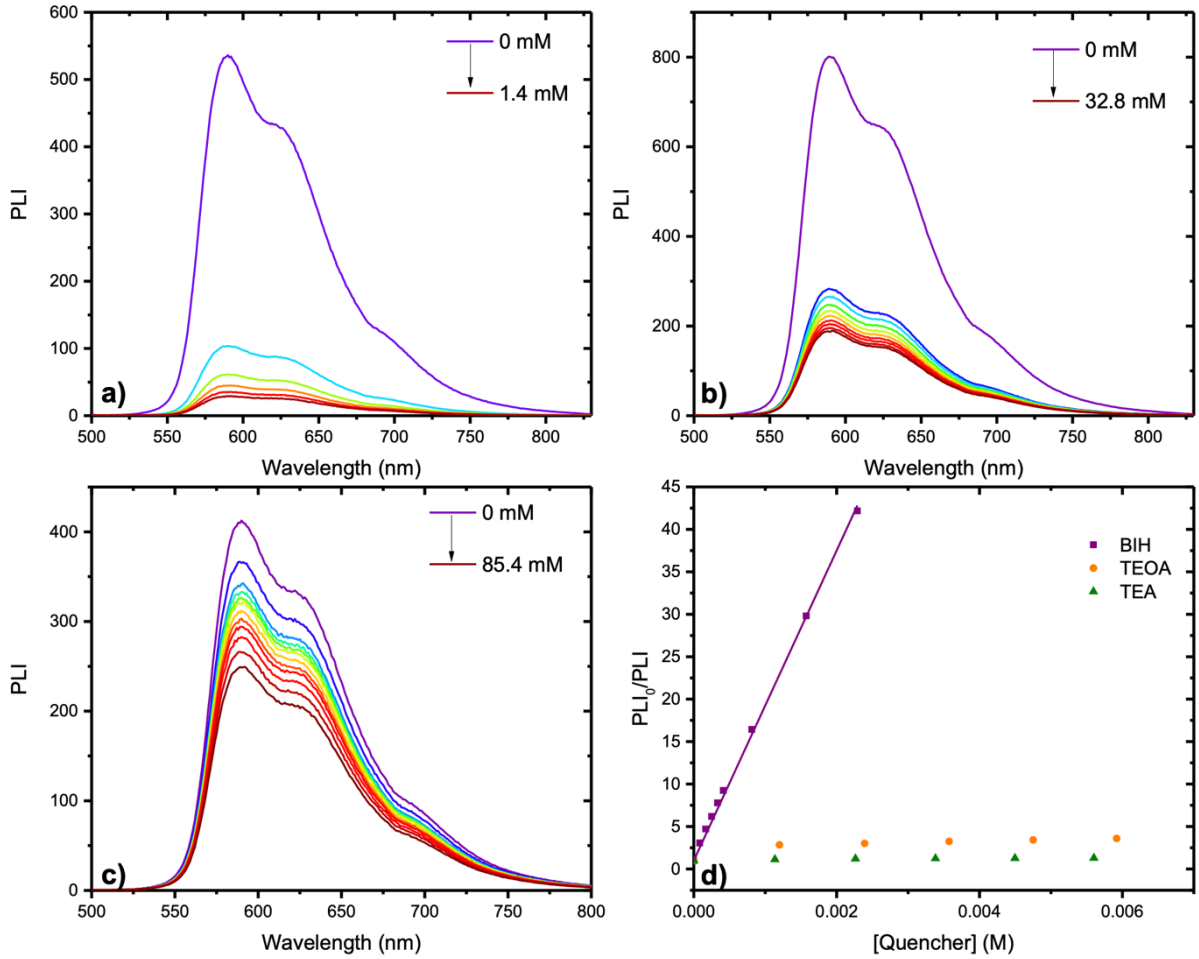

Figure S12. Excited-state quenching of $[Ir(piq)_2(bpy)]^+$ with BIH (a), TEOA (b) and TEA (c) in argon purged acetonitrile. The corresponding Stern-Volmer plots is shown in panel d, with the corresponding linear fit for the excited-state quenching in the presence of BIH.

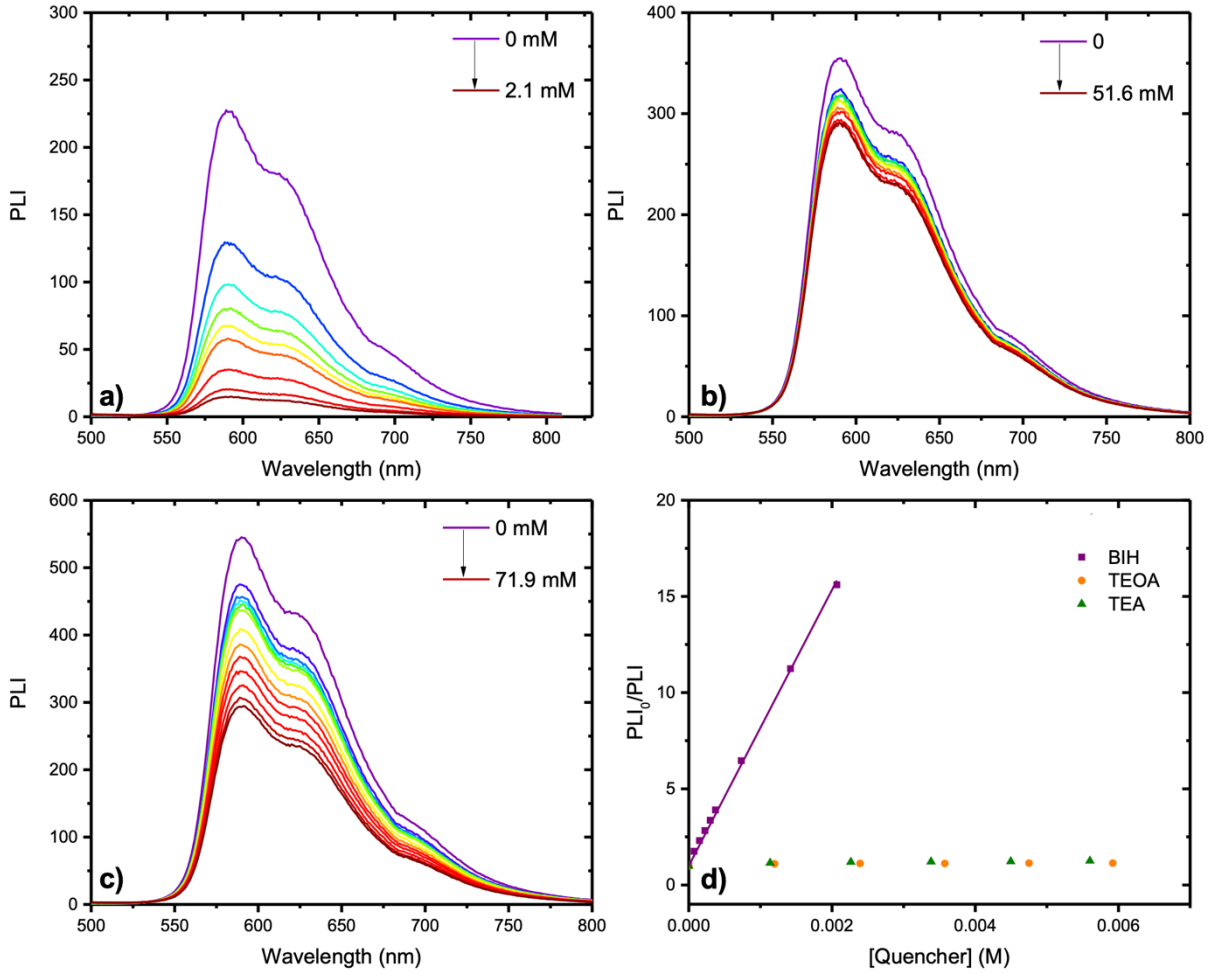

Figure S13. Excited-state quenching of $[Ir(piq)_2(4,4'\text{-}(^tBu)_2\text{-}bpy)]^+$ with BIH (a), TEOA (b) and TEA (c) in argon purged acetonitrile. The corresponding Stern-Volmer plots is shown in panel d, with the corresponding linear fit for the excited-state quenching in the presence of BIH.

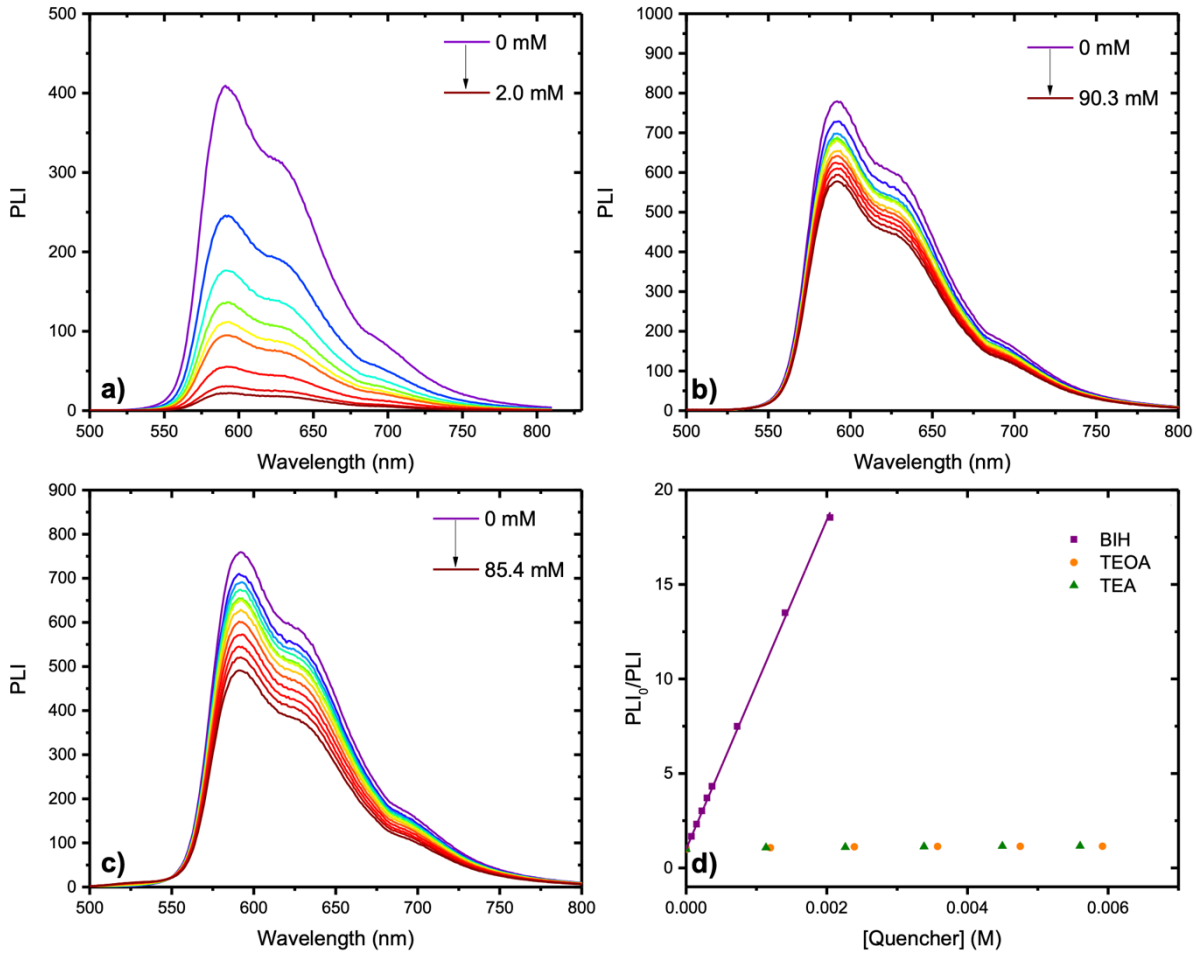

Figure S14. Excited-state quenching of $[Ir(piq)_2(4,4'\text{-}(OCH_3)_2\text{-}bpy)]^+$ with BIH (a), TEOA (b) and TEA (c) in argon purged acetonitrile. The corresponding Stern-Volmer plots is shown in panel d, with the corresponding linear fit for the excited-state quenching in the presence of BIH.

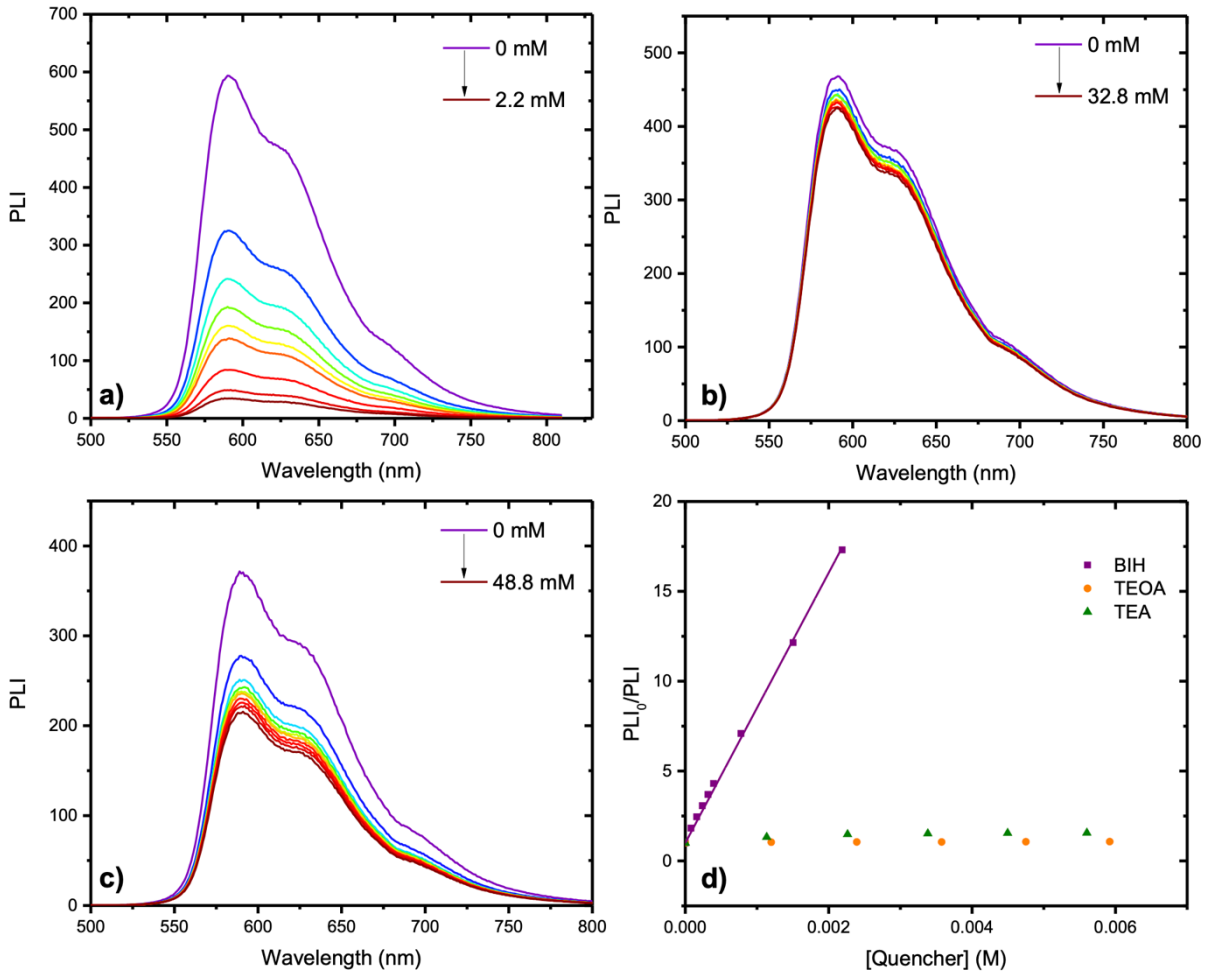

Figure S15. Excited-state quenching of $[Ir(piq)_2(4,4'\text{-}(C_9H_{19})_2\text{-}bpy)]^+$ with BIH (a), TEOA (b) and TEA (c) in argon purged acetonitrile. The corresponding Stern-Volmer plots is shown in panel d, with the corresponding linear fit for the excited-state quenching in the presence of BIH.

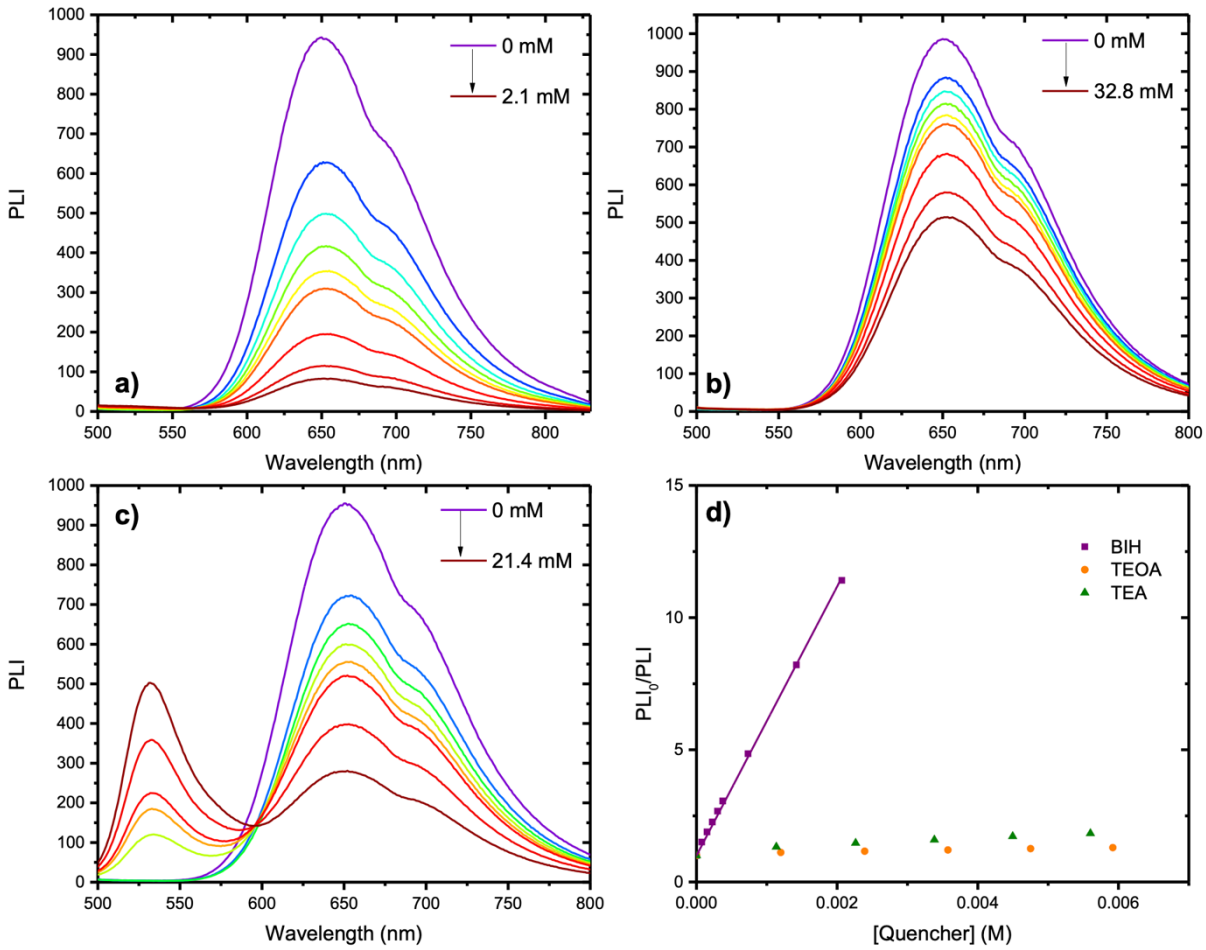

Figure S16. Excited-state quenching of $[Ir(piq)_2(biq)]^+$ with BIH (a), TEOA (b) and TEA (c) in argon purged acetonitrile. The corresponding Stern-Volmer plots is shown in panel d, with the corresponding linear fit for the excited-state quenching in the presence of BIH.

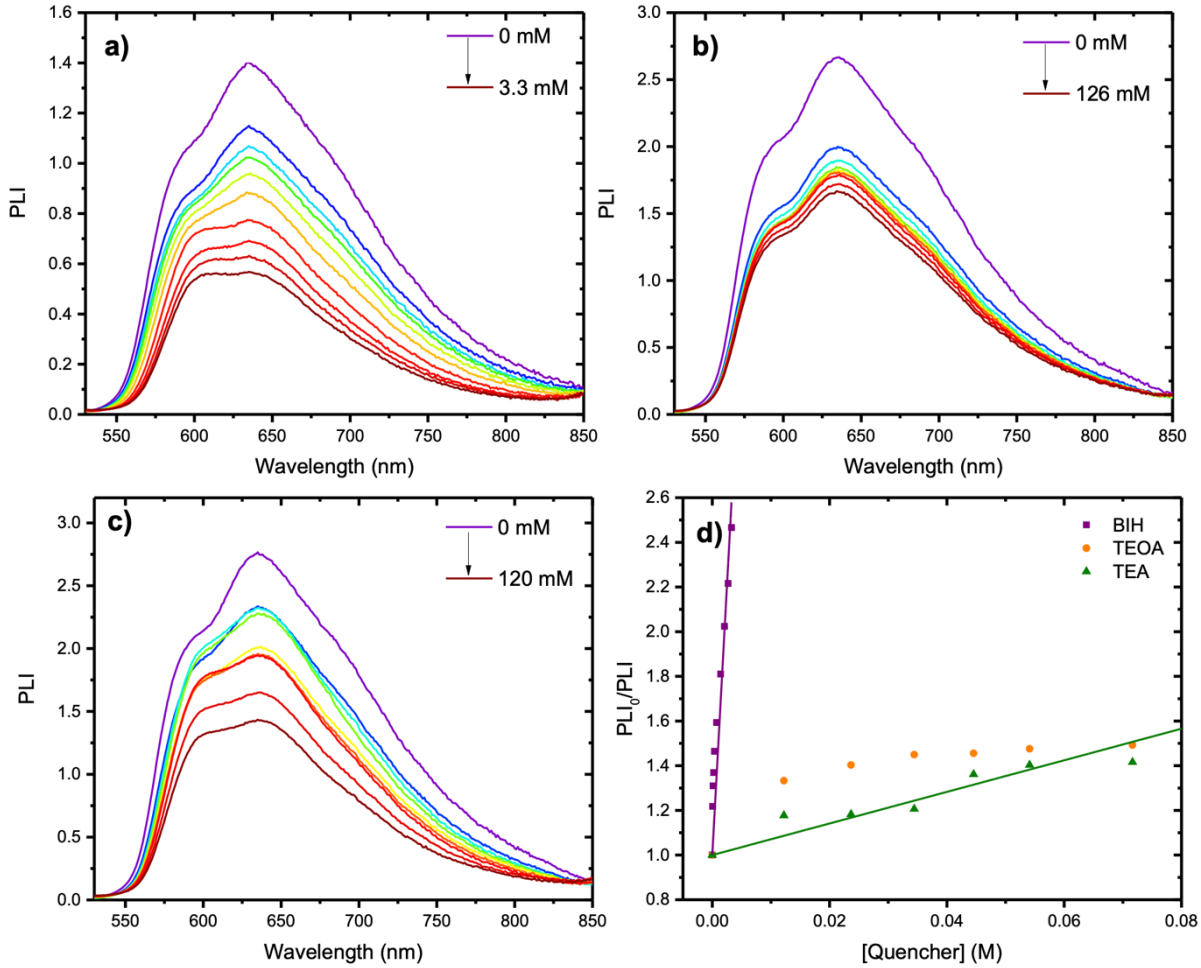

Figure S17. Excited-state quenching of $[Ir(piq)_2(4,4'\text{-}(Br)_2\text{-}bpy)]^+$ with BIH (a), TEOA (b) and TEA (c) in argon purged acetonitrile. The corresponding Stern-Volmer plots is shown in panel d, with the corresponding linear fit for the excited-state quenching in the presence of BIH.

Steady-State Photolysis

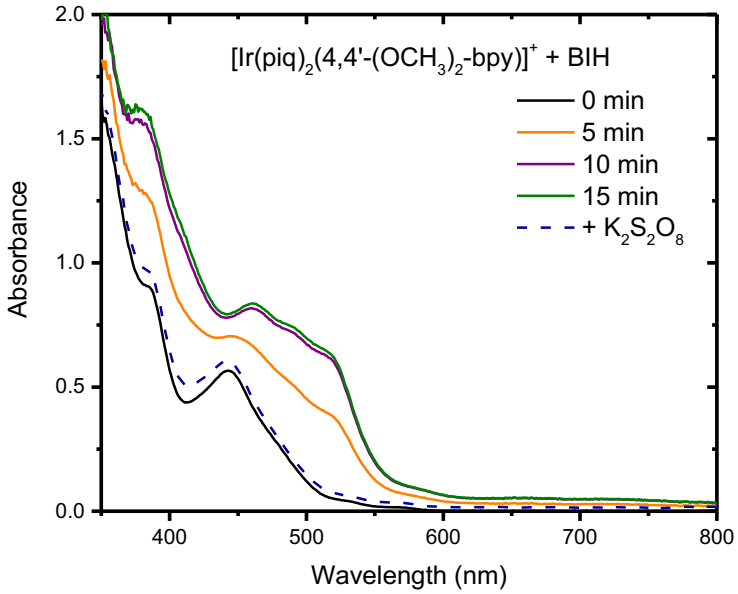

Figure S18. Absorption spectra of $[Ir(piq)_2(4,4'\text{-}(OCH_3)_2\text{-}bpy)]^+$ in argon-purged acetonitrile at room temperature at t= 0 minutes (black) and following 5 minutes (orange), 10 minutes (purple) and 15 minutes (olive) irradiation with blue-light in the presence of 1 mM BIH. After the experiment, $K_2S_2O_8$ was added to oxidize the photo-reduced photosensitizer and investigate reversibility.

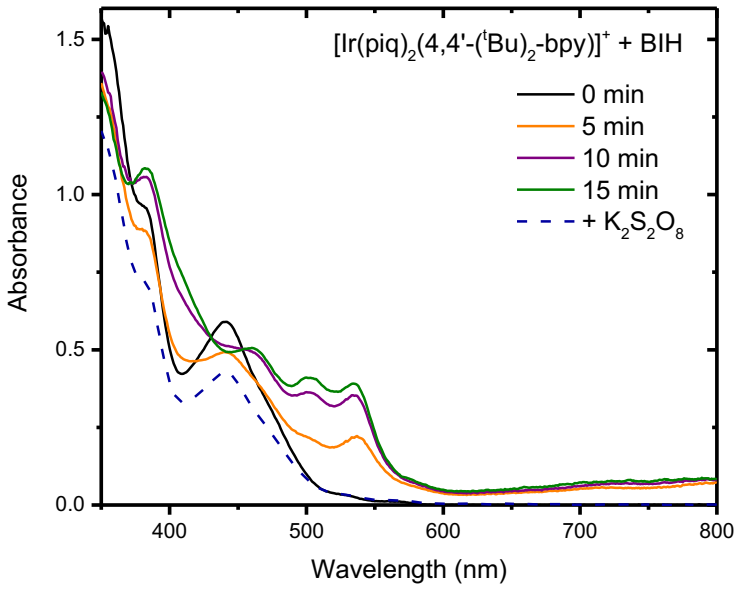

Figure S19. Absorption spectra of $[Ir(piq)_2(4,4'\text{-}(^tBu)_2\text{-}bpy)]^+$ in argon-purged acetonitrile at room temperature at t= 0 minutes (black) and following 5 minutes (orange), 10 minutes (purple) and 15 minutes (olive) irradiation with blue-light in the presence of 1 mM BIH. After the experiment, $K_2S_2O_8$ was added to oxidize the photo-reduced photosensitizer and investigate reversibility.

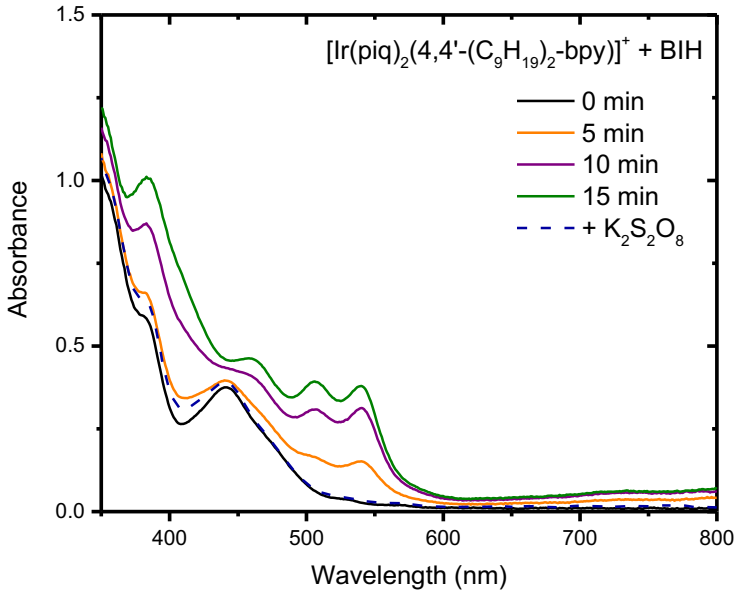

Figure S20. Absorption spectra of $[Ir(piq)_2(4,4'\text{-}(C_9H_{19})_2\text{-}bpy)]^+$ in argon-purged acetonitrile at room temperature at t= 0 minutes (black) and following 5 minutes (orange), 10 minutes (purple) and 15 minutes (olive) irradiation with blue-light in the presence of 1 mM BIH. After the experiment, $K_2S_2O_8$ was added to oxidize the photo-reduced photosensitizer and investigate reversibility.

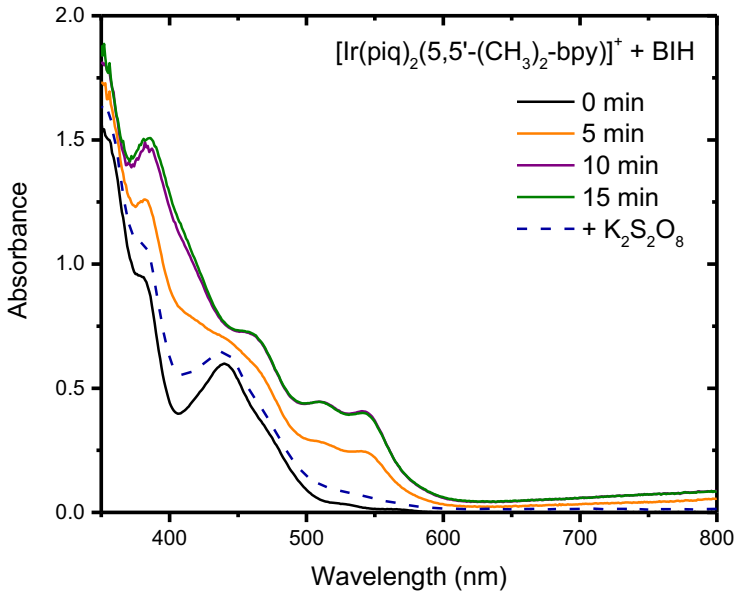

Figure S21. Absorption spectra of $[Ir(piq)_2(5,5'\text{-}(CH_3)_2\text{-}bpy)]^+$ in argon-purged acetonitrile at room temperature at t= 0 minutes (black) and following 5 minutes (orange), 10 minutes (purple) and 15 minutes (olive) irradiation with blue-light in the presence of 1 mM BIH. After the experiment, $K_2S_2O_8$ was added to oxidize the photo-reduced photosensitizer and investigate reversibility.

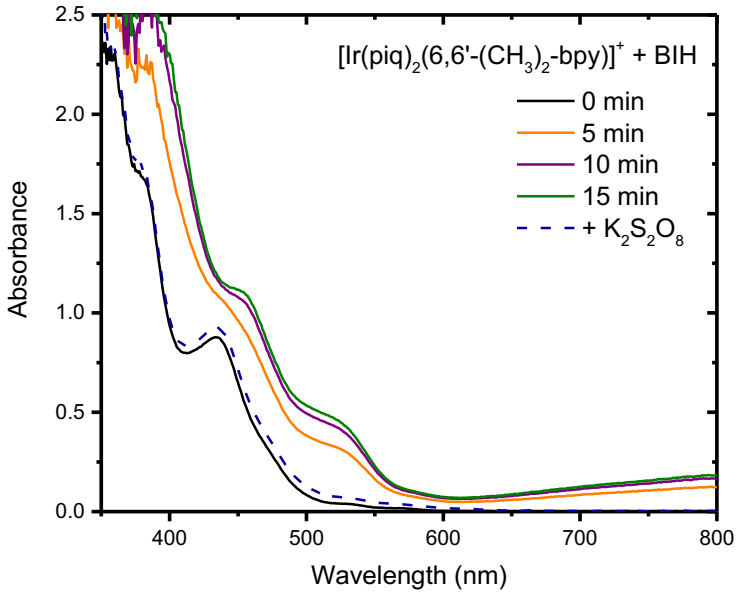

Figure S22. Absorption spectra of $[Ir(piq)_2(6,6'\text{-}(CH_3)_2\text{-}bpy)]^+$ in argon-purged acetonitrile at room temperature at t= 0 minutes (black) and following 5 minutes (orange), 10 minutes (purple) and 15 minutes (olive) irradiation with blue-light in the presence of 1 mM BIH. After the experiment, $K_2S_2O_8$ was added to oxidize the photo-reduced photosensitizer and investigate reversibility.

High-Resolution Mass Spectrometry

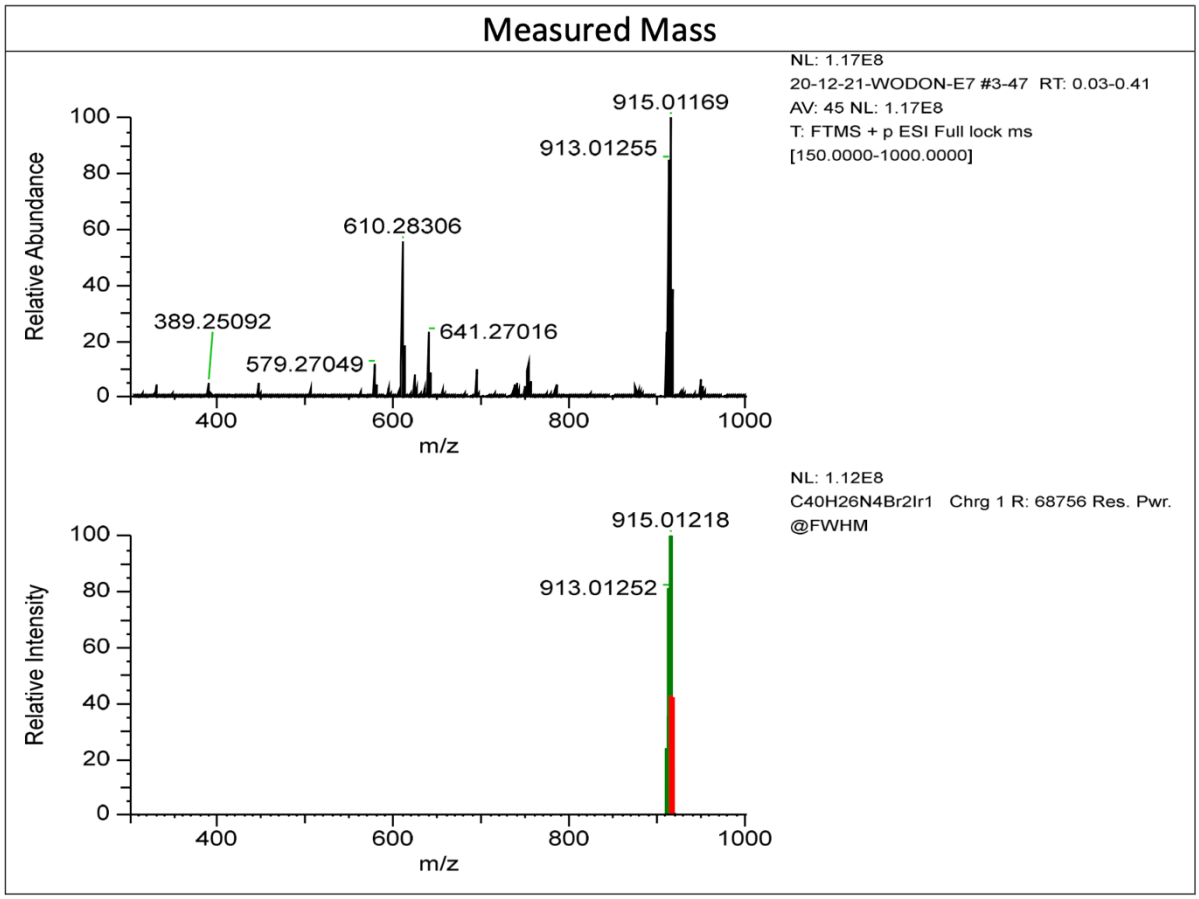

Elemental Composition Results

Peak Mass	Display Formula	MS Cov. [%]	Delta [ppm]	Theo. mass
911.01276	$C_{40}H_{28}N_4{}^{79}Br_2{}^{191}Ir$	99.97	0.33	911.01246

Figure S23. High-resolution mass spectrum of $[Ir(piq)_2(4,4'\text{-}(Br)_2\text{-}bpy)]^+$.

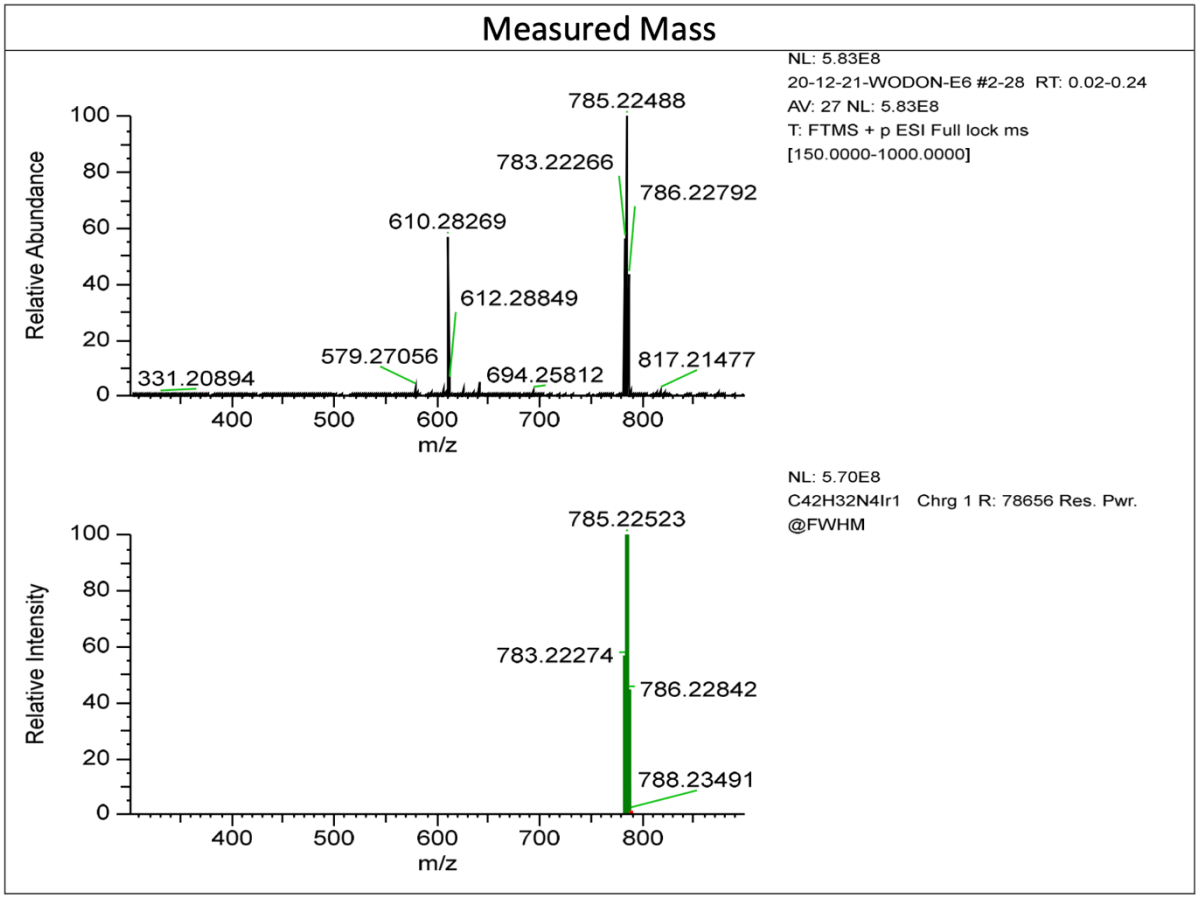

Elemental Composition Results

Peak Mass	Display Formula	MS Cov. [%]	Delta [ppm]	Theo. mass
783.22266	$C_{42}H_{32}N_4{}^{191}Ir$	99.84	-0.10	783.22274

Figure S24. High-resolution mass spectrum of $[Ir(piq)_2(4,4'\text{-}(CH_3)_2\text{-bpy})]^+$.

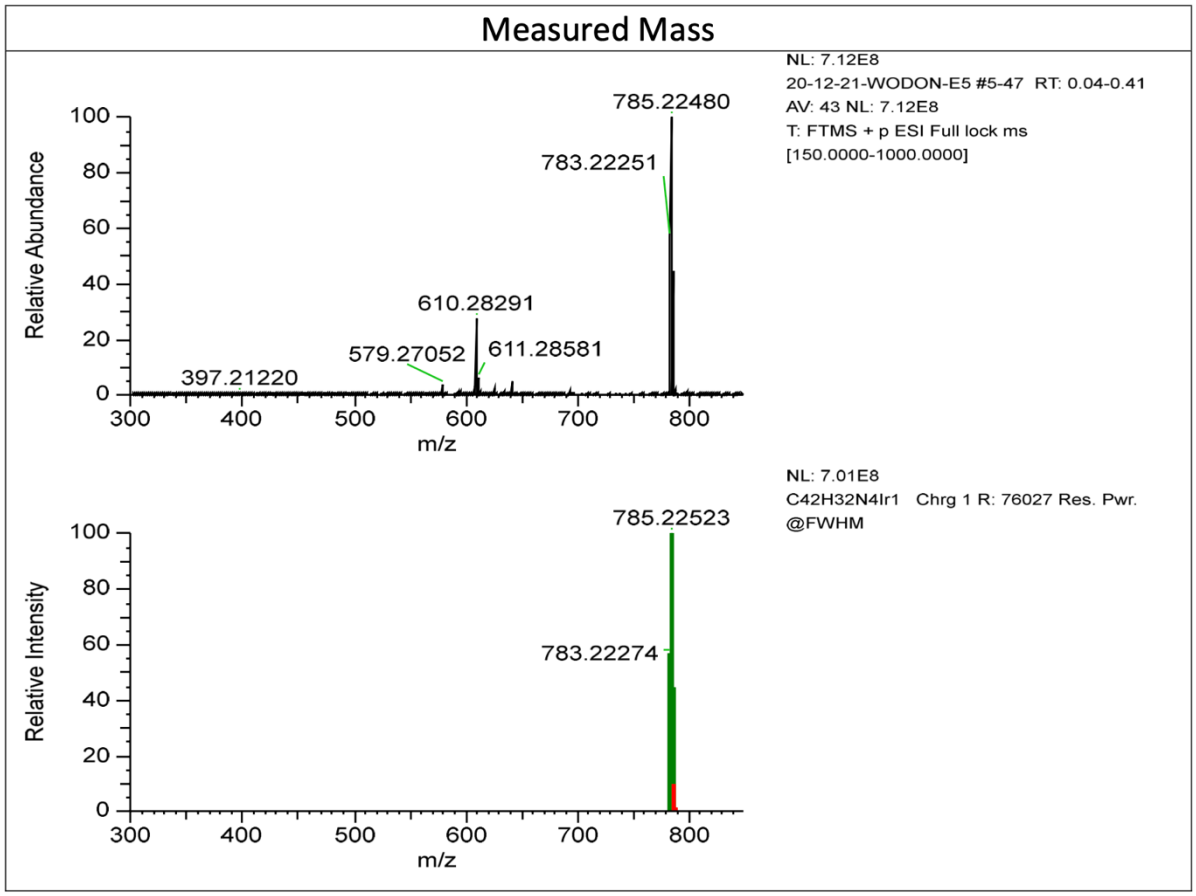

Elemental Composition Results

Peak Mass	Display Formula	MS Cov. [%]	Delta [ppm]	Theo. mass
783.22251	$C_{42}H_{32}N_4{}^{191}Ir$	99.89	-0.29	783.22274

Figure S25. High-resolution mass spectrum of $[Ir(piq)_2(5,5'\text{-}(CH_3)_2\text{-bpy})]^+$.

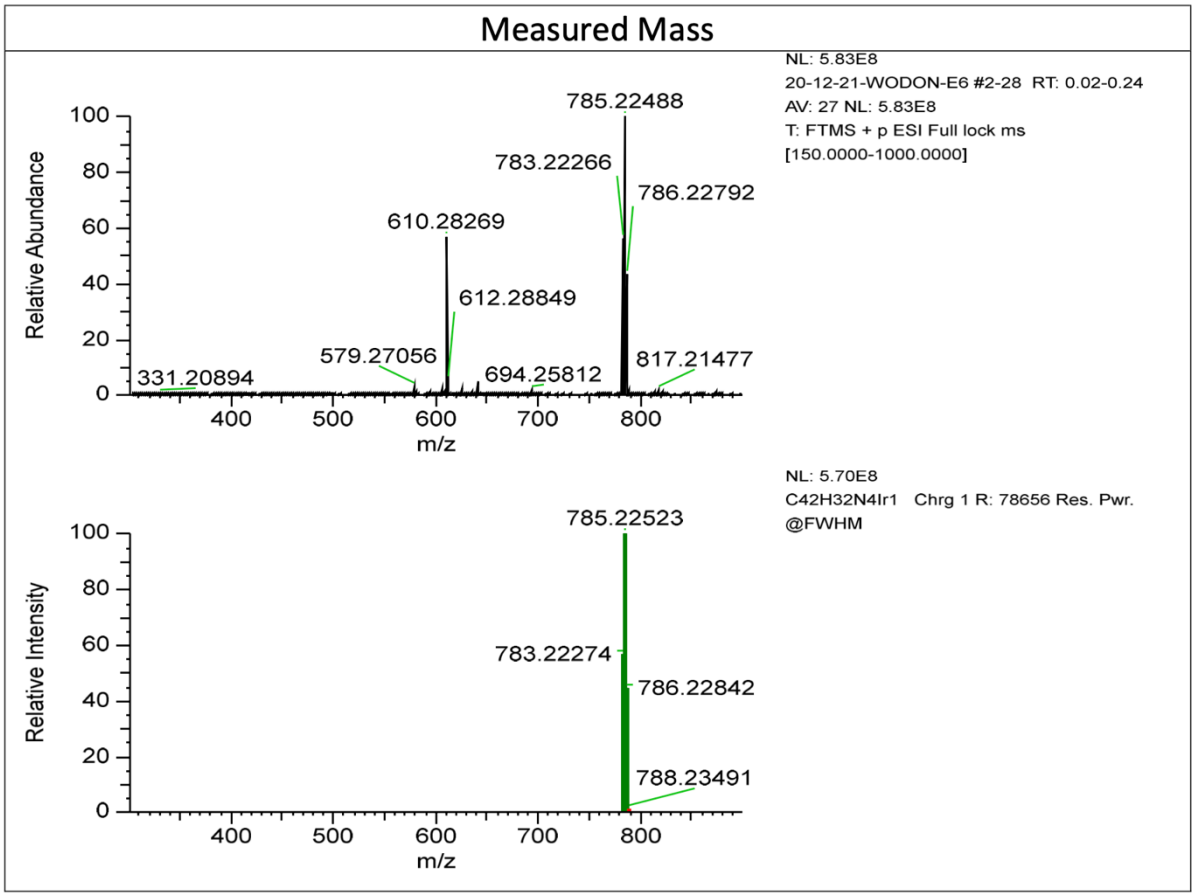

Elemental Composition Results

Peak Mass	Display Formula	MS Cov. [%]	Delta [ppm]	Theo. mass
783.22256	$C_{42}H_{32}N_4{}^{191}Ir$	99.71	-0.23	783.22274

Figure S26. High-resolution mass spectrum of $[Ir(piq)_2(6,6'\text{-}(CH_3)_2\text{-bpy})]^+$.

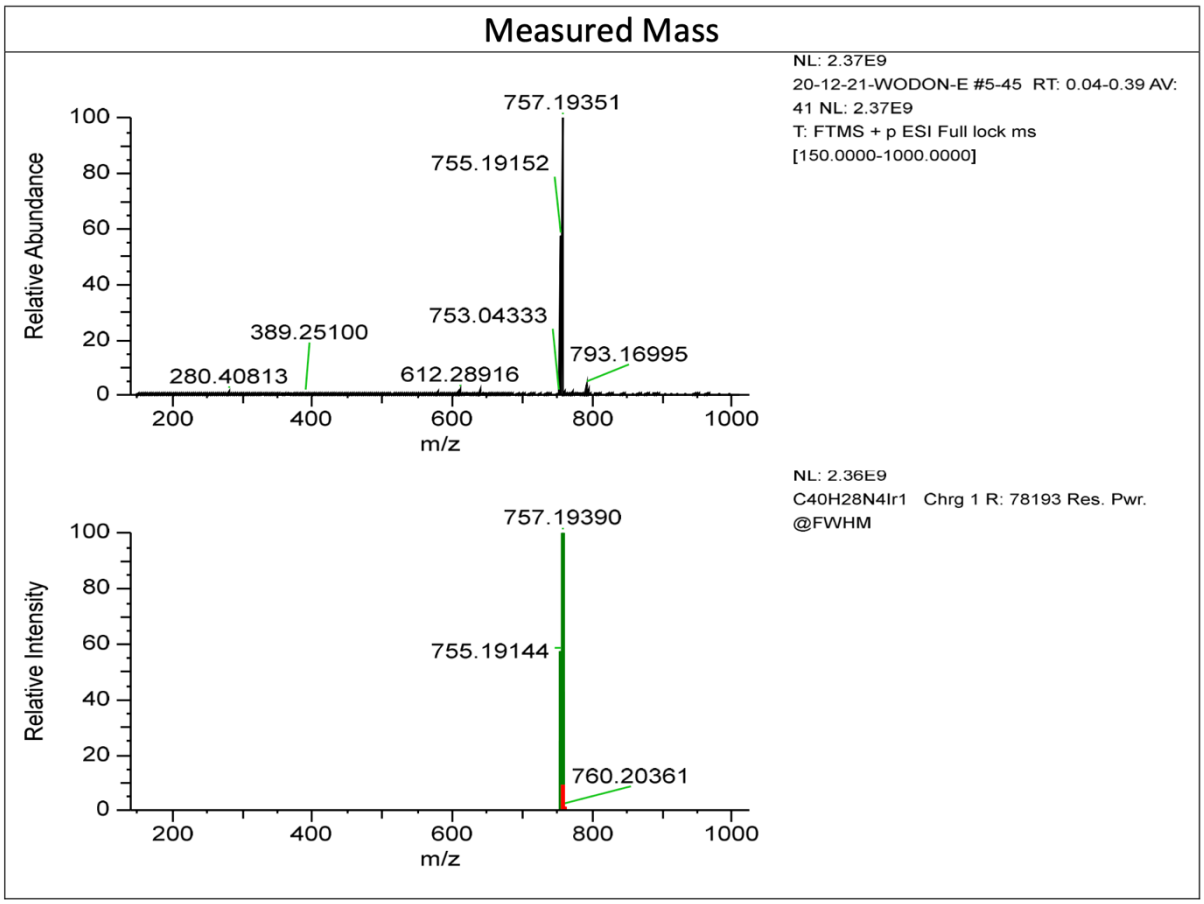

Elemental Composition Results

Peak Mass	Display Formula	MS Cov. [%]	Delta [ppm]	Theo. mass
755.19152	$C_{40}H_{28}N_4{}^{191}Ir$	99.73	0.10	755.19144

Figure S27. High-resolution mass spectrum of $[Ir(piq)_2(bpy)]^+$.

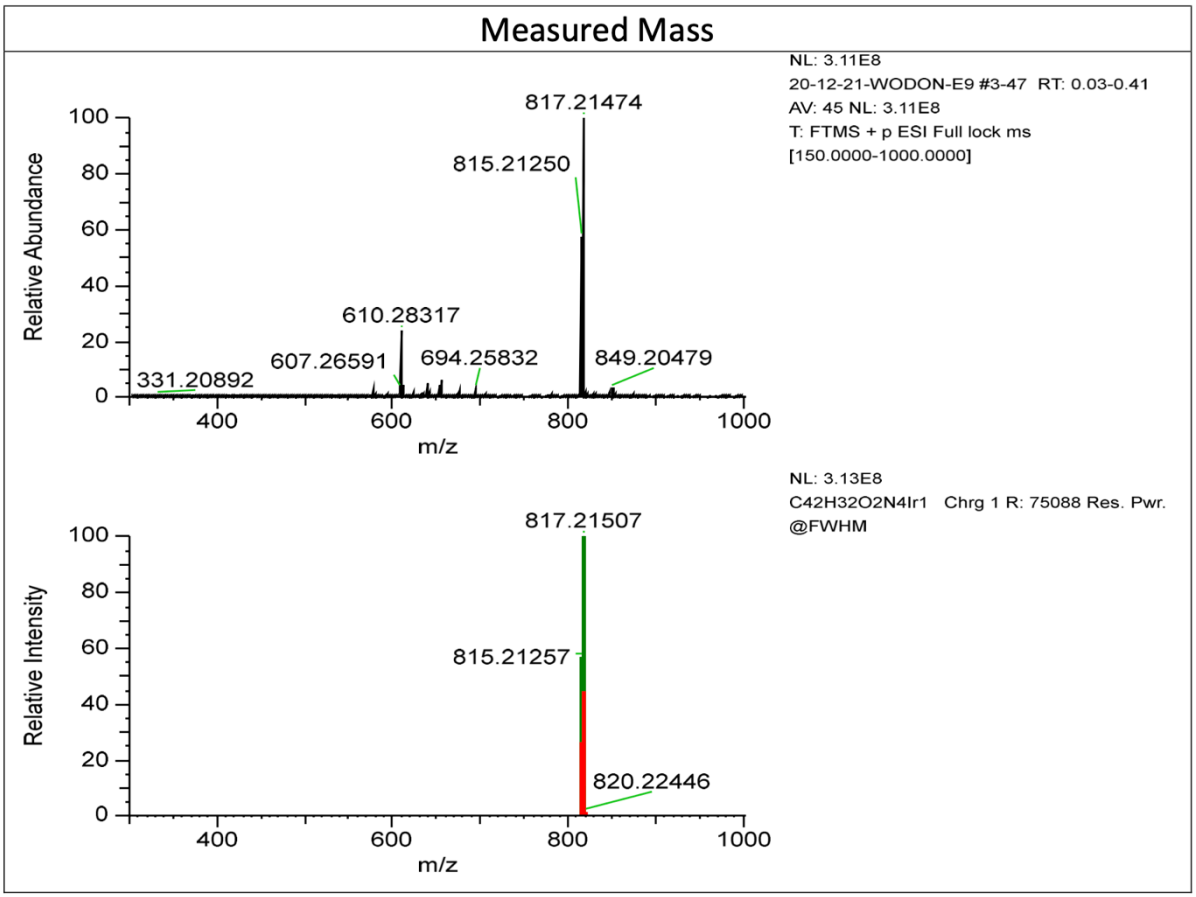

Elemental Composition Results

Peak Mass	Display Formula	MS Cov. [%]	Delta [ppm]	Theo. mass
815.21250	$C_{42}H_{32}O_2N_4{}^{191}Ir$	99.65	-0.09	815.21257

Figure S28. High-resolution mass spectrum of $[Ir(piq)_2(4,4'\text{-}(OCH_3)_2\text{-}bpy)]^+$.

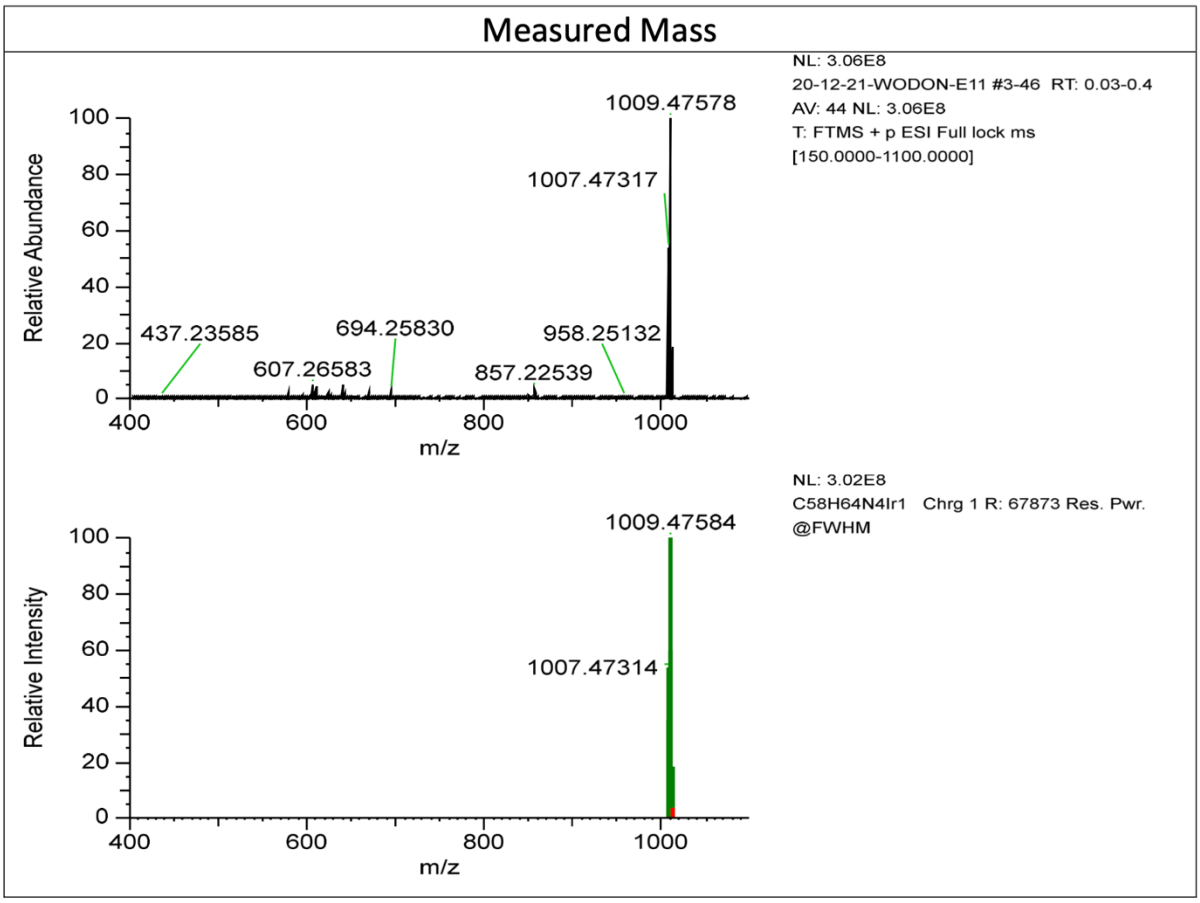

Elemental Composition Results

Peak Mass	Display Formula	MS Cov. [%]	Delta [ppm]	Theo. mass
1007.47317	$C_{58}H_{64}N_4{}^{191}Ir$	99.97	0.03	1007.47314

Figure S29. High-resolution mass spectrum of $[Ir(piq)_2(4,4'\text{-}(C_9H_{19})_2\text{-bpy})]^+$.

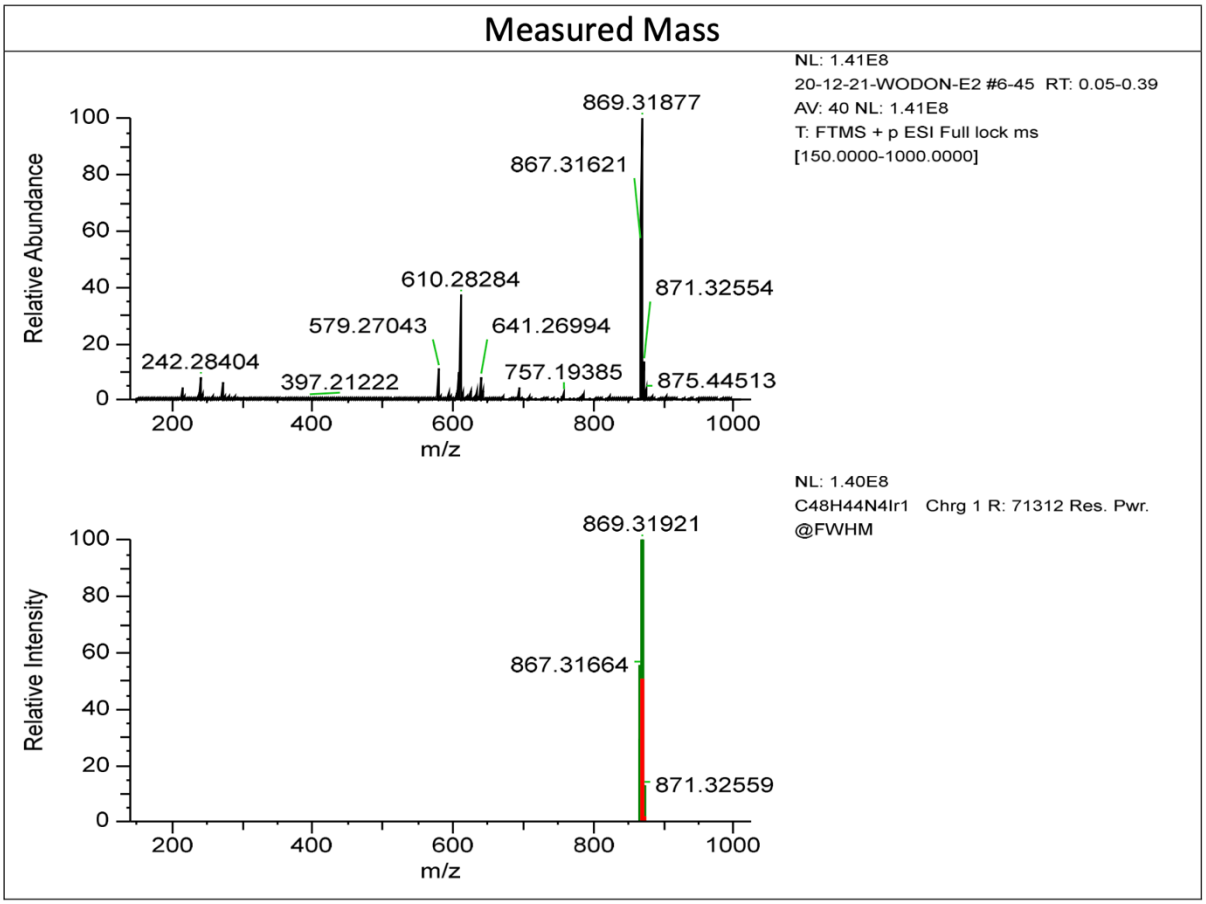

Elemental Composition Results

Peak Mass	Display Formula	MS Cov. [%]	Delta [ppm]	Theo. mass
867.31621	$C_{48}H_{44}N_4{}^{191}Ir$	99.97	-0.49	867.31664

Figure S30. High-resolution mass spectrum of $[Ir(piq)_2(4,4'\text{-}(^t Bu)_2\text{-bpy})]^+$.

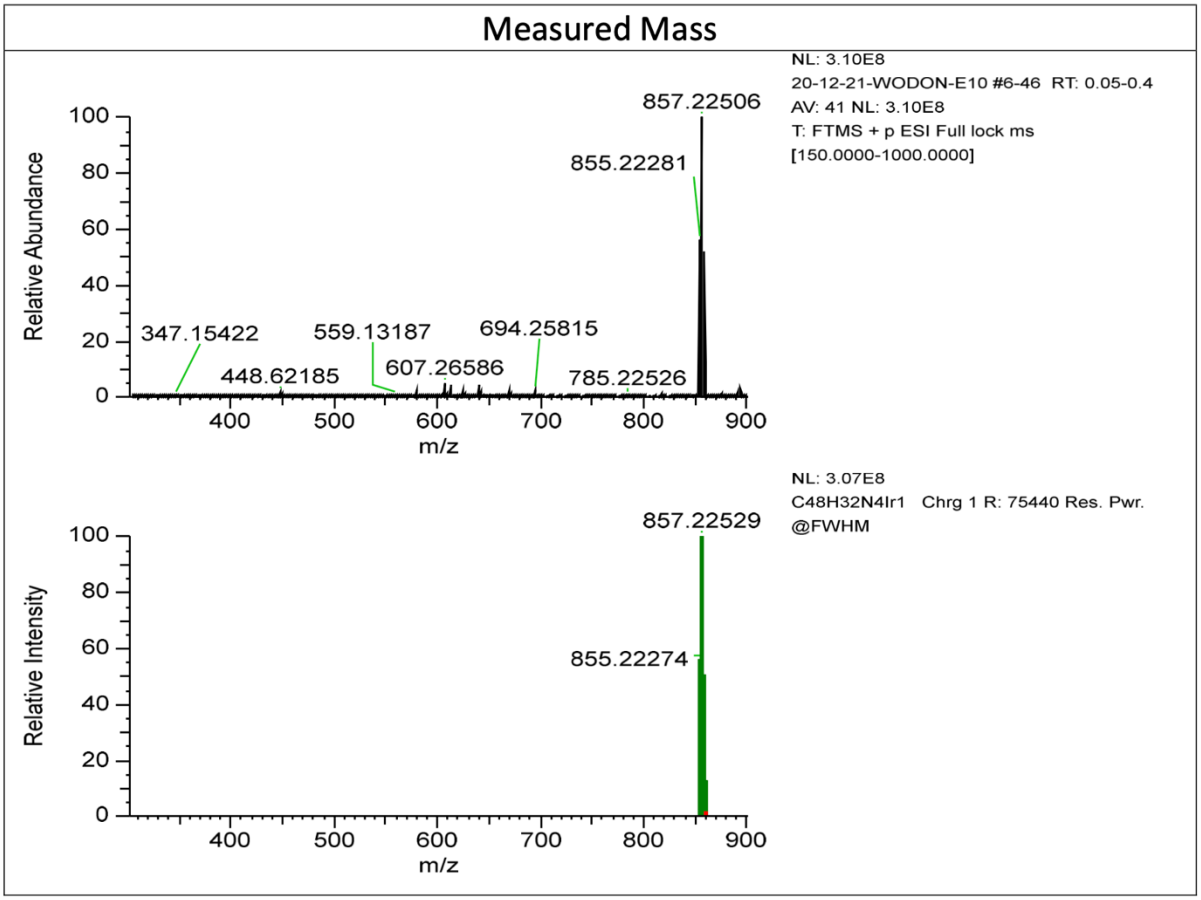

Elemental Composition Results

Peak Mass	Display Formula	MS Cov. [%]	Delta [ppm]	Theo. mass
855.22281	$C_{48}H_{32}N_4{}^{191}Ir$	99.94	0.08	855.22274

Figure S31. High-resolution mass spectrum of $[Ir(piq)_2(biq)]^+$.

^{1}H NMR Spectra

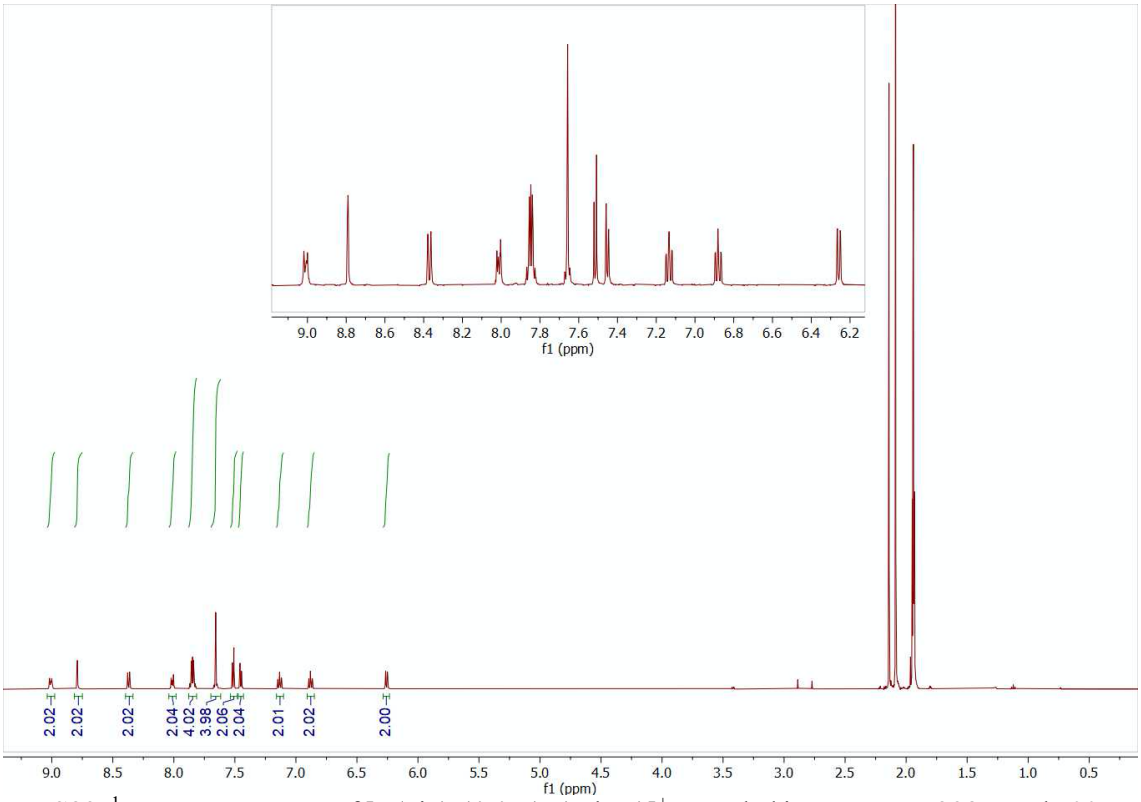

Figure S32. ^{1}H NMR spectrum of $[Ir(piq)_2(4,4'\text{-}(Br)_2\text{-}bpy)]^+$ recorded in CD_3CN at 298K and 500 MHz.

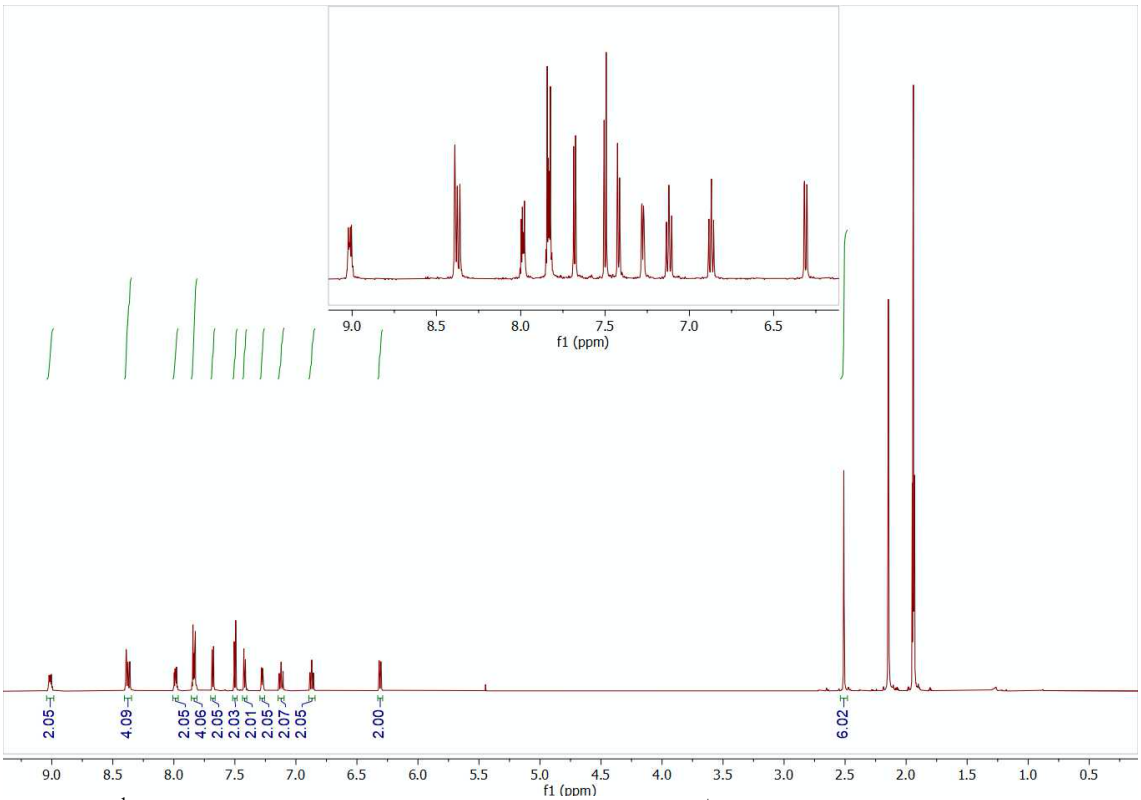

Figure S33. ^{1}H NMR spectrum of $[Ir(piq)_2(4,4'\text{-}(CH_3)_2\text{-}bpy)]^+$ recorded in CD_3CN at 298K and 500 MHz.

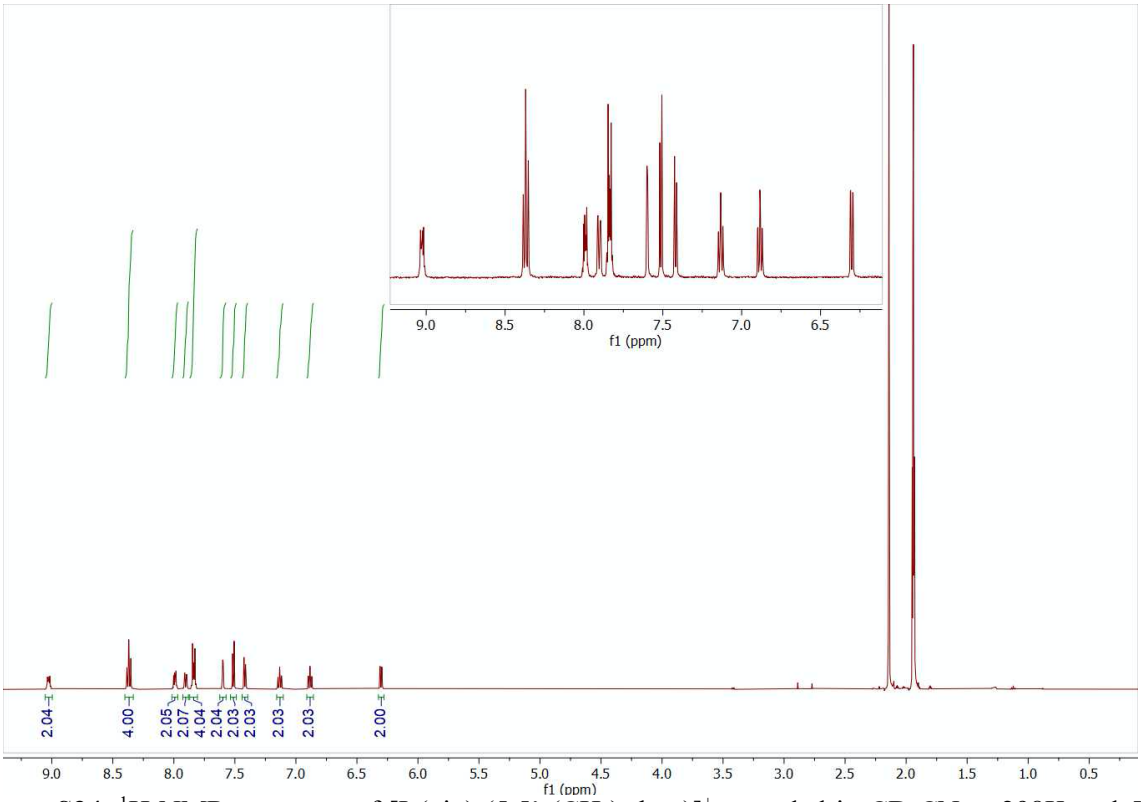

Figure S34. ^{1}H NMR spectrum of $[Ir(piq)_2(5,5'\text{-}(CH_3)_2\text{-bpy})]^+$ recorded in CD_3CN at 298K and 500 MHz.

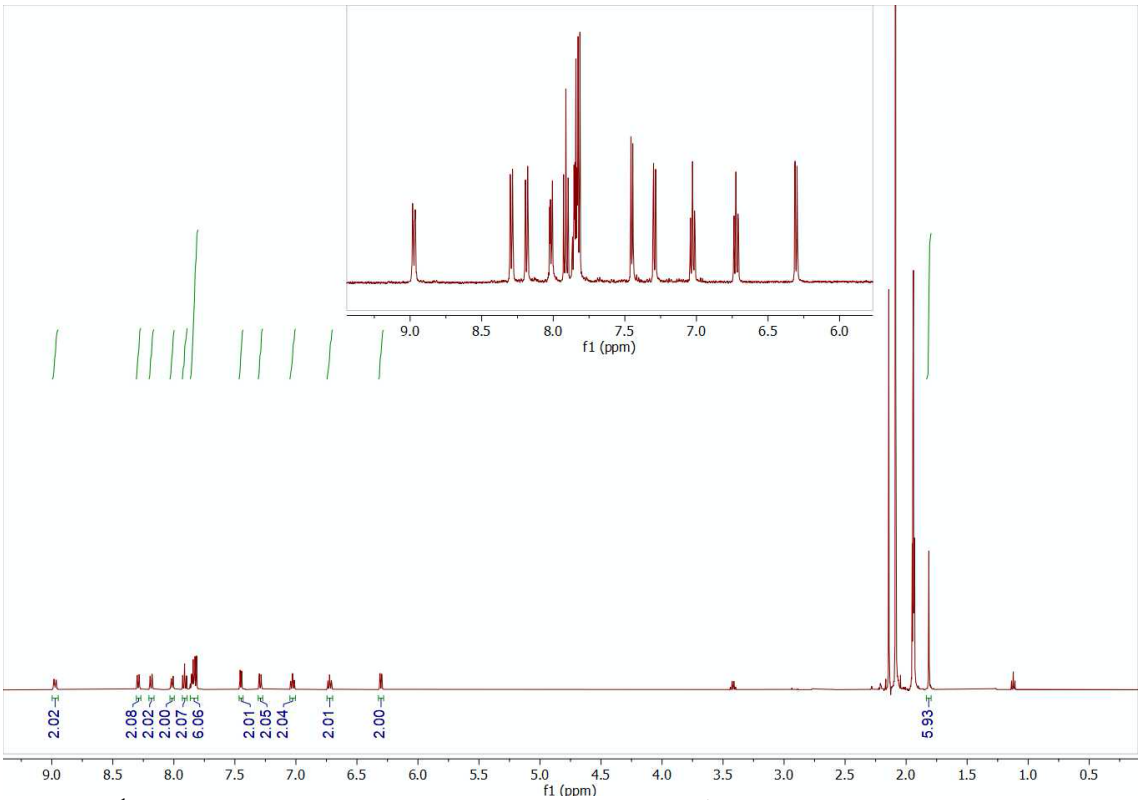

Figure S35. ^{1}H NMR spectrum of $[Ir(piq)_2(6,6'\text{-}(CH_3)_2\text{-bpy})]^+$ recorded in CD_3CN at 298K and 500 MHz.

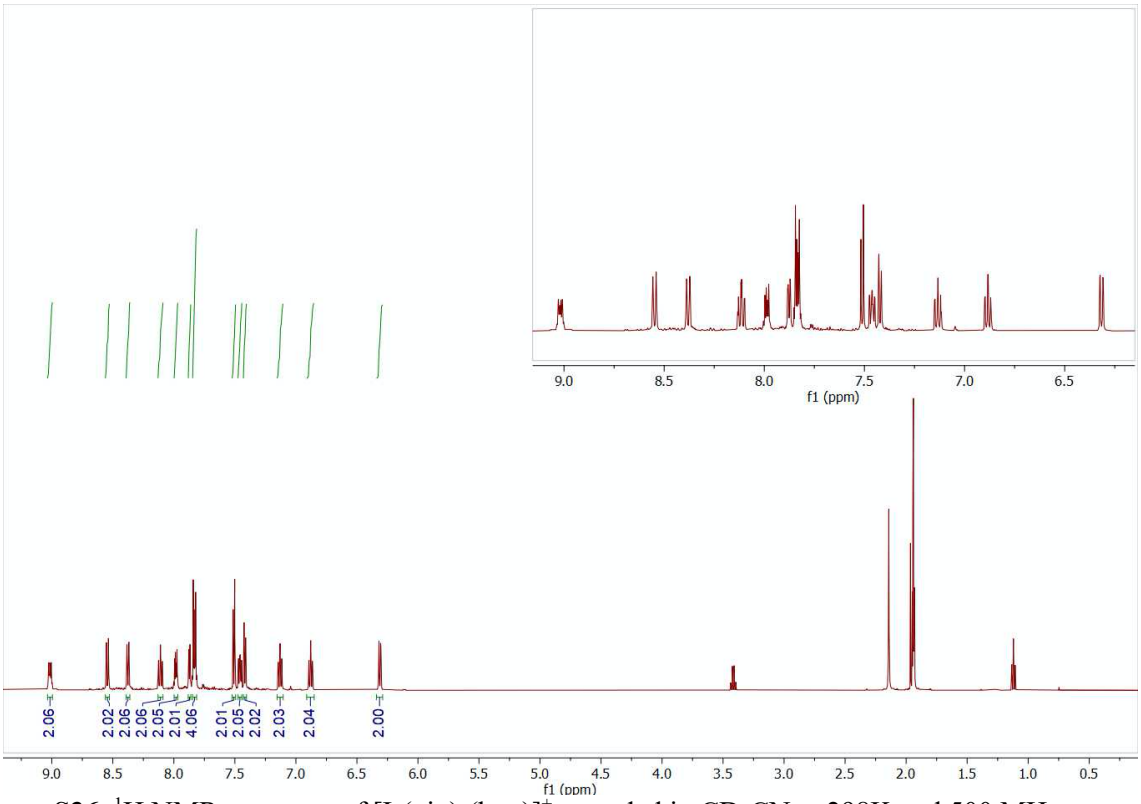

Figure S36. ^{1}H NMR spectrum of $[Ir(piq)_2(bpy)]^+$ recorded in CD_3CN at 298K and 500 MHz.

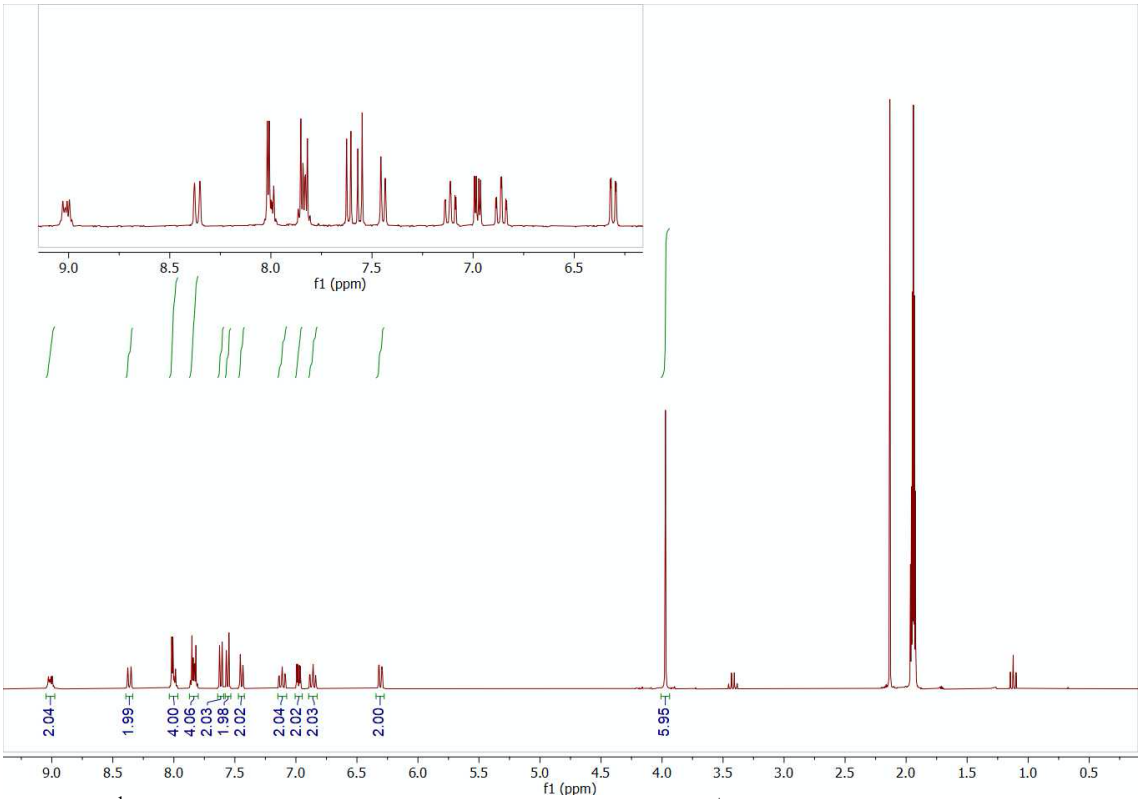

Figure S37. ^{1}H NMR spectrum of $[Ir(piq)_2(4,4'\text{-}(OCH_3)_2\text{-}bpy)]^+$ recorded in CD_3CN at 298K and 500 MHz.

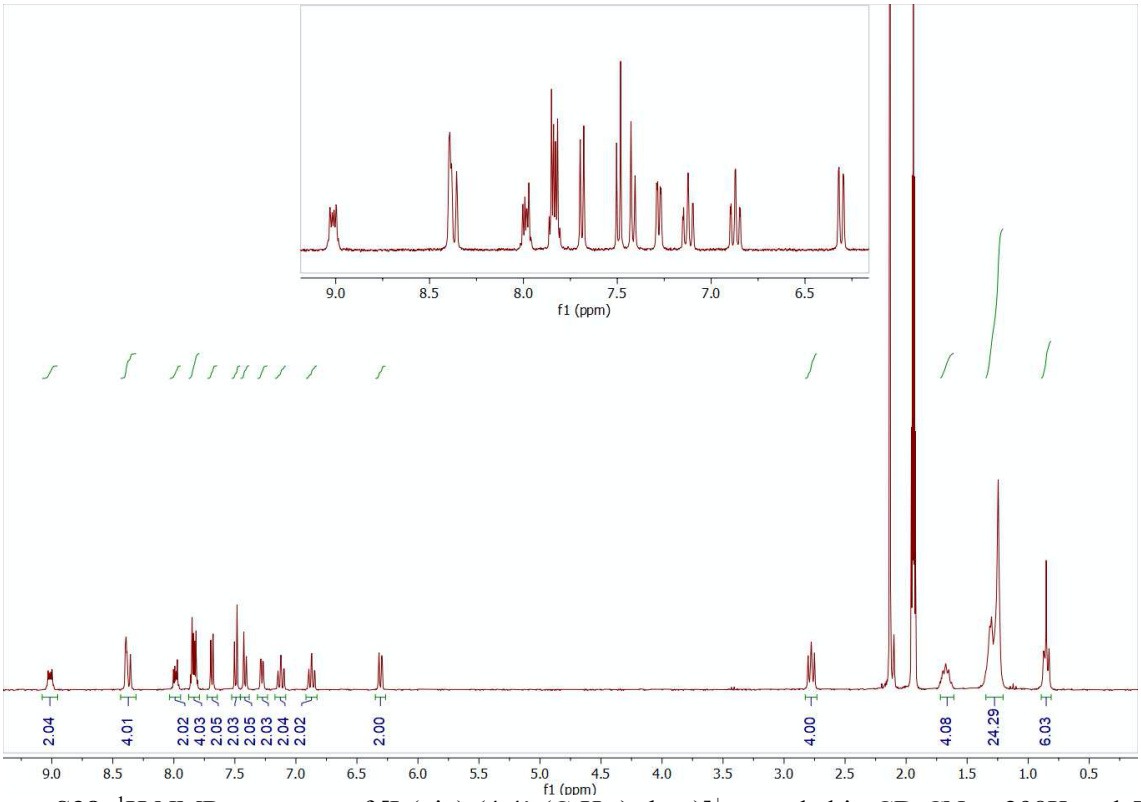

Figure S38. ^{1}H NMR spectrum of $[Ir(piq)_2(4,4'\text{-}(C_9H_{19})_2\text{-bpy})]^+$ recorded in CD_3CN at 298K and 500 MHz.

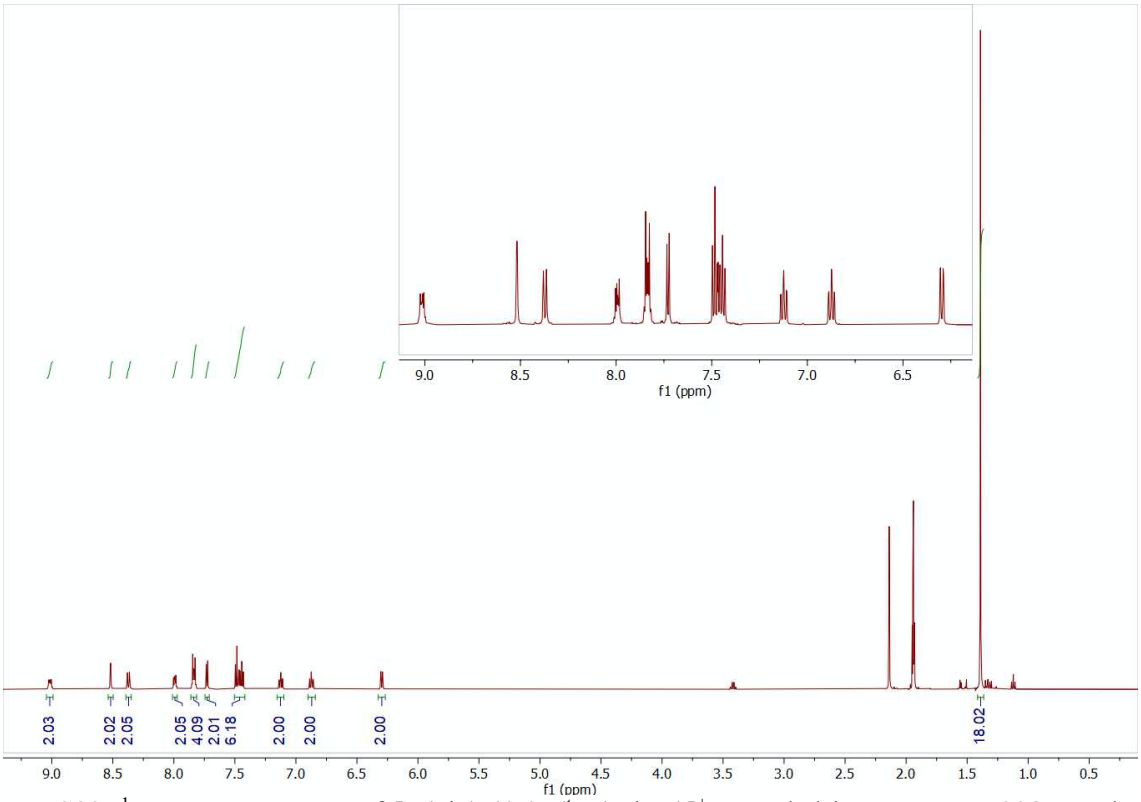

Figure S39. ^{1}H NMR spectrum of $[Ir(piq)_2(4,4'\text{-}(^{t}Bu)_2\text{-bpy})]^+$ recorded in CD_3CN at 298K and 500 MHz.

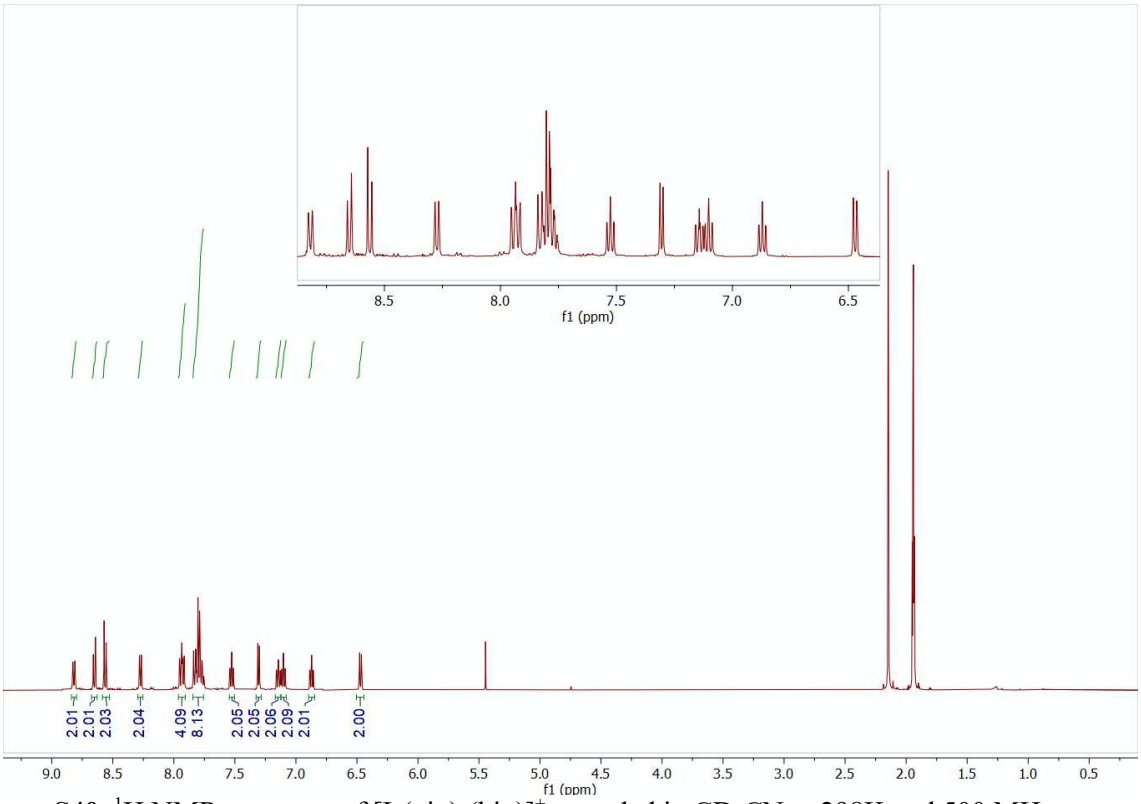

Figure S40. ^{1}H NMR spectrum of $[Ir(piq)_2(biq)]^+$ recorded in CD_3CN at 298K and 500 MHz.

Accumulation of Mono-Reduced $[Ir(piq)_2(LL)]^+$ Photosensitizers Relevant for Solar Fuels Productions

A series of nine $[Ir(piq)_2(LL)]^+.PF_6^-$ photosensitizers were developed and investigated for excited-state electron transfer with sacrificial electron donors that included triethanolamine (TEOA), triethylamine (TEA), and 1,3-dimethyl-2-phenyl-2,3-dihydro-1*H*-benzo[*d*]imidazole (BIH) in acetonitrile. The photosensitizers were obtained in 57-82% yield starting from the common $[Ir(piq)_2Cl]_2$ precursor and were all characterized by UV-Vis absorption as well as by steady-state, time-resolved spectroscopies, and electrochemistry. The excited-state lifetimes ranged from 250 to 3350 ns and were also shown, in some cases, to be strongly influenced by dissolved oxygen. Excited-state electron transfer quenching rate constants in the 10 $M^{-1}s^{-1}$ range were obtained when BIH was used as electron donor. These quenching rate constants were three orders of magnitude higher than when TEA or TEOA is used. Steady-state photolysis in the presence of BIH showed that the stable and reversible accumulation of mono-reduced photosensitizers was possible, highlighting the potential use of these Ir-based photosensitizers in photocatalytic reactions relevant for solar fuels production.

Auteur: Martin Wodon

UNIVERSITE CATHOLIQUE DE LOUVAIN
Faculté bioingénieurs
Croix du sud, 2 bte L7.05.01, 1348 Louvain-la-Neuve, Belgique I **www.uclouvain.be/agro**